APPLICATIONS AND ADAPTATIONS OF A GLOBALLY CONVERGENT NUMERICAL METHOD IN INVERSE PROBLEMS

by

AUBREY RHODEN

Presented to the Faculty of the Graduate School of

The University of Texas at Arlington in Partial Fulfillment

of the Requirements

for the Degree of

DOCTOR OF PHILOSOPHY

THE UNIVERSITY OF TEXAS AT ARLINGTON

May 2013

To my brother West, my cousin Jacob, my daughter Jude, and my nephews Quinn and Glenn.

ACKNOWLEDGEMENTS

I would like to acknowledge and extend my heartfelt gratitude to my supervising professor Dr. Jianzhong Su for his constant motivation, encouragement and for making the completion of this dissertation possible.

I also wish to thank Dr. Benito Chen, Dr. Ren-Cang Li, Dr. Hristo V. Kojouharov and Dr. Gaik Ambartsoumian for their invaluable support and for taking time to serve on my dissertation committee.

I am grateful to all the teachers who taught me during the years I spent at Texas State University and the University of Texas at Arlington. I also would like to thank several of my friends who have supported me throughout my education.

Finally, I would like to express my deep gratitude to my mother Melissa, my father Neal, my brothers West and Madison, my sister Olivia and my wife Ginna who have encouraged and inspired me.

April 19, 2013

ABSTRACT

APPLICATIONS AND ADAPTATIONS OF A GLOBALLY CONVERGENT NUMERICAL METHOD IN INVERSE PROBLEMS

AUBREY RHODEN, Ph.D.

The University of Texas at Arlington, 2013

Supervising Professor: Jianzhong Su

In our terminology "globally convergent numerical method" means a numerical method whose convergence to a good approximation of the correct solution is independent of the initial approximation in inverse problems. A numerical imaging algorithm has been proposed to solve a coefficient inverse problem for an elliptic equation and then the algorithm is validated with the data generated by computer simulation. Previous work in this field was focused on the steady-state optical problem with multiple source positions moving along a straight line as well as the frequency domain problem with sweeping frequency. This work includes the steady-state thermal tomography problem with multiple source positions moving along a straight line as well as the time-dependent optical tomography problem using only two fixed source positions. A convergence analysis shows that this method converges globally assuming the smallness of the asymptotic solution (the so-called tail function). A heuristic approach for approximating the "new tail-function" has been utilized and verified in numerical experiments, so has the global convergence. Numerical experiments in the 2D time-dependent optical and steady-state thermal property reconstruction are presented.

TABLE OF CONTENTS

LIST OF ILLUSTRATIONS

LIST OF TABLES

CHAPTER 1

INTRODUCTION

1.1 Introduction of Inverse Problem

In our terminology "globally convergent numerical method for Inverse Problems" means a numerical method, whose convergence to a good approximation for the correct solution by starting from any initial approximation is guaranteed by mathematical proof. This is fundamentally different from other current methods for commonly used locally convergent numerical methods, the phenomenon of multiple local minima and ravines of least squares residual functions represent the major obstacle for reliable numerical solutions of Coefficient Inverse Problems (CIPs) for Partial Differential Equations (PDEs). To assure that we approximate the true solution close enough, the issue of addressing the problem of local minima has *vital importance* for this discipline. Indeed, any gradient-like optimization method of such a functional would likely converge to a local minimum located far from the correct solution. The vast majority of current numerical method for CIPs are locally convergent ones, like, for example Newton-like method, see, e.g., [1][2][3][4] and their references within. That is, convergence of such a method to the true solution is rigorously guaranteed only if the initial guess is located sufficiently close to that solution. However, in the majority of applications such as medical and military ones, the optical media of interest is highly heterogeneous, which means that a good first guess is not available. The latter naturally raises the question about the reliability of locally convergent numerical method for those applications, and this question is well known to many practitioners working on computations of real world Inverse Problems.

Thus, we are interested in the issue of globally convergent numerical methods for CIPs. We call a numerical method globally convergent if the following two conditions are in place: (1) a rigorous convergence analysis ensures that this method leads to a good approximation of the true solutions regardless of the availability of a first good guess, and (2) numerical experiments confirm the said convergence properly.

In this paper we present a globally convergent method for a CIP for the equation

$$-w_t(\boldsymbol{x},t)+\Delta w(\boldsymbol{x},t)-a(\boldsymbol{x})w(\boldsymbol{x},t)=0,\quad \boldsymbol{x}\in\mathbb{R}^2, t>0 \tag{1.1}$$

where $w(\boldsymbol{x},0)=\delta(\boldsymbol{x}-\boldsymbol{x}_0)$ and

$$\lim_{|\boldsymbol{x}|\to\infty} w(\boldsymbol{x},t)=0\,. \tag{1.2}$$

Here w is the light or heat intensity and x_0 is the point source position that generates the illuminating light or heat for the inverse problem. We assume throughout this paper that the function $a(\boldsymbol{x})\in C^{\alpha}(\mathbb{R}^2)$, $a(\boldsymbol{x})\geq$ const. >0 where $\alpha\in(0,1)$. Uniqueness and existence of the solution of the problem (1.1) and (1.2) is such that $w\in C^{2+\alpha}(|\boldsymbol{x}-\boldsymbol{x}_0|\geq\varepsilon)$, for all $\varepsilon>0$ follows from classic arguments, see [5] for further reference.

In previous work [6][7][8], the global convergence is rigorously proven by assuming that we know a good approximation for the tail-function, i.e. we assume that we know a good approximation of the fourth term of the asymptotic behavior of the function $\ln[w(\boldsymbol{x},\boldsymbol{x}_0)]$ for $|\boldsymbol{x}_0|\to\infty$, equation (7.4) in [9]. The new algorithm which uses time-resolved measurement data of light intensity is less dependent on a large number of source positions since a single source position will have a range of pseudo-frequencies. However the new challenge is that the GCM formulation becomes much more complex and the time-domain data needs a more precise time-gated intensified charged coupled device (ICCD) camera.

This type of GCM that uses the asymptotic behavior of the PDE to solve the inverse problem has applications to other PDE's as long as the asymptotic behavior is known. It has been applied to the inverse problem involving the wave equation where the intention is to recover relative dielectric permativity to detect dielectric abnormalities, see [10].

1.2 Applications

1.2.1 Diffuse Optical Tomography (DOT)

In diffuse optical tomography there are several types of light sources used to probe the light absorption and scattering media. The first application of the DOT is in optical medical imaging of tumor-like abnormalities both in human organs and small animals using near-infrared (NIR) light with the wavelength of light somewhere between 500 and 1000 nm [11]. The second feasible application is in optical imaging of targets on battlefields via smog and flames using propagation of light originated by lasers. Both cases of transmitted and back reflected light are feasible in applications. Interestingly, the diffuse-like propagation of light would be helpful, because the direct light can miss the target, one might still image it because photons would still 'sense' that target due to the diffusion of the light. We refer to [1] for an in-depth review of the field. It should be noted this is a low resolution method. So multi-modalities incorporating high resolution techniques such as ultrasound, MRI, or X-ray could be useful, see [12].

1.2.2 Thermal Tomography

In medical imaging it is often useful to calculate blood perfusion rates within the body for diagnosing many conditions including tumors, blood clots, etc. One of the applications of this method is in thermal tomography where the governing equation

is a form Penne's bio-heat transfer equation where the change with respect to time is considered negligible if the temperature had reached a state of equilibrium, see references [13][14]. Let $w(\boldsymbol{x}, \boldsymbol{x}_0)$ represent the temperature, the governing equation would be

$$-w_t(\boldsymbol{x}, \boldsymbol{x}_0) + k\Delta w(\boldsymbol{x}, \boldsymbol{x}_0) + W_b(\boldsymbol{x})c_b(w_a - w(\boldsymbol{x}, \boldsymbol{x}_0)) = -Q_m - \delta(\boldsymbol{x} - \boldsymbol{x}_0) \tag{1.3}$$

which reaches thermal equilibrium at

$$\Delta w(\boldsymbol{x}, \boldsymbol{x}_0) - a(\boldsymbol{x})w(\boldsymbol{x}, \boldsymbol{x}_0)) = -Q_m - \delta(\boldsymbol{x} - \boldsymbol{x}_0) - a(\boldsymbol{x})w_a \tag{1.4}$$

where

$$a(\boldsymbol{x}) = \frac{W_b(\boldsymbol{x})c_b}{k} \tag{1.5}$$

The coefficients c_b - specific heat and k - thermal conductivity are considered constant while W_b the blood perfusion rate is a function of space. $\delta(\boldsymbol{x} - \boldsymbol{x}_0)$ is a heat source function located at x_0. The metabolic heat generated Q_m becomes negligible with the addition of the heat source, and the addition of the arterial temperature w_a is compensated for by the Dirichlet boundary condition that $w_a = 36.9$ degrees Celsius on the outer boundary. So that our new thermal equation has the same form as the optical tomography equation.

$$\Delta w(\boldsymbol{x}, \boldsymbol{x}_0) - a(\boldsymbol{x})w(\boldsymbol{x}, \boldsymbol{x}_0) = -\delta(\boldsymbol{x} - \boldsymbol{x}_0) \tag{1.6}$$

Of course Penne's bio-heat transfer equation was originally designed to govern heat transfer through blood flow treating the body as a closed circulatory system that delivers heat. In our case we are not considering an entire system with vessels and arteries, but rather trying to reconstruct the perfusion qualities of an almost uniform piece of flesh that contains possibly several inclusions that are decreasing the body temperature in a reasonable fashion.

CHAPTER 2

MATHEMATICAL MODEL OF THE STEADY-STATE PROBLEM

We rewrite equation (1.6) to depend on $\boldsymbol{x}$ and s as follows:

$$\Delta w(\boldsymbol{x}, s) - a(\boldsymbol{x}) w(\boldsymbol{x}, s) = -\delta(x - B, y - s), \tag{2.1}$$

$$\lim_{|\boldsymbol{x}| \to \infty} w(\boldsymbol{x}, s) = 0\,. \tag{2.2}$$

The inverse problem

Denote $\boldsymbol{x} = (x, y)$. Let $\Omega \subset \mathbb{R}^2$ be a bounded domain and $\Gamma = \partial\Omega$. Let B be a constant. Determine the coefficient $a(\boldsymbol{x})$ in equation (2.1) for $\boldsymbol{x} \in \Omega$, assuming that the following function $\varphi(\boldsymbol{x}, s)$ is given

$$w(\boldsymbol{x}, s) = \varphi(\boldsymbol{x}, s), \qquad \forall \boldsymbol{x} \in \Gamma, \quad \forall s \in [\underline{s}, \overline{s}], \tag{2.3}$$

where $\overline{s}$ is a sufficient large number, $\underline{s} < \overline{s}$ is a certain fixed number and

$$\{\boldsymbol{x}_0 \in (s, B), s \geq \underline{s}\} \cap \overline{\Omega} = \varnothing\,.$$

Figure (2.1) shows the geometry of the inverse problem.

2.1 Nonlinear Integral Differential Equation

Since the source $\boldsymbol{x}_0 = (B, s) \notin \Omega$ and our inverse problem is performed in Ω domain, equation (2.1) can be written as

$$\Delta w(\boldsymbol{x}, s) - a(\boldsymbol{x}) w(\boldsymbol{x}, s) = 0, \quad \boldsymbol{x} \in \Omega. \tag{2.4}$$

Function w is positive by the maximum principle, so we can consider the function $u = \ln w$ and obtain the following equation from equation (2.4)

$$\Delta u(\boldsymbol{x}, s) + [\nabla u(\boldsymbol{x}, s)]^2 = a(\boldsymbol{x}), \tag{2.5}$$

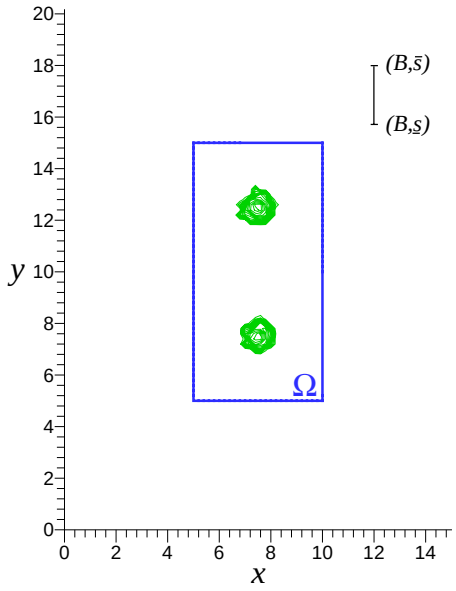

Figure 2.1. The geometry of the steady-state inverse problem, . .

$$u(\boldsymbol{x}, s) = \phi(\boldsymbol{x}, s) \quad \forall\ (\boldsymbol{x}, s) \in \Gamma \times (\underline{s}, \overline{s})\,, \tag{2.6}$$

where $\phi = \ln \varphi$.

This dissertation is focused on the technique of making the tail-function small as in the globally convergent numerical methods [15]. Accordingly we deduce another form of the inverse problem as following. Let

$$v(\boldsymbol{x}, s) = \frac{u(\boldsymbol{x}, s)}{s^2}\,. \tag{2.7}$$

Equation (2.5) becomes

$$\Delta v(\boldsymbol{x}, s) + s^2[\nabla v(\boldsymbol{x}, s)]^2 = \frac{a(\boldsymbol{x})}{s^2} \tag{2.8}$$

Denote

$$q(\boldsymbol{x}, s) = \frac{\partial}{\partial s} v(\boldsymbol{x}, s)\,. \tag{2.9}$$

We have

$$\Delta q(\boldsymbol{x}, s) + 2s^2 \nabla q(\boldsymbol{x}, s) \cdot \nabla v(\boldsymbol{x}, s) + 2s[\nabla v(\boldsymbol{x}, s)]^2 = -2\frac{a(\boldsymbol{x})}{s^3}\,, \tag{2.10}$$

$$\boldsymbol{x} \in \Omega\,, \quad s \in (\underline{s}, \overline{s}]$$

where

$$v(\boldsymbol{x}, s) = -\int_s^{\overline{s}} q(\boldsymbol{x}, \tau)\, d\tau + v(\boldsymbol{x}, \overline{s})\,, \quad \boldsymbol{x} \in \Omega\,, \quad s \in [\underline{s}, \overline{s}] \tag{2.11}$$

where $\overline{s}$ is a large number which will be chosen in numerical experiments. The new small tail-function in equation (2.11) is obtained by

$$v(\boldsymbol{x}, \overline{s}) = \frac{u(\boldsymbol{x}, \overline{s})}{\overline{s}^2}\,. \tag{2.12}$$

We obtain from equations (2.8), (2.10) and (2.11) the following "Nonlinear Integral Differential Equation"

$$\Delta q + 2s^2 \nabla q \cdot \left(-\int_s^{\overline{s}} \nabla q\, d\tau + \nabla \bar{v} \right) + 4s \left(-\int_s^{\overline{s}} \nabla q\, d\tau + \nabla \bar{v} \right)^2 = -\frac{2}{s} \left(-\int_s^{\overline{s}} \Delta q\, d\tau + \Delta \bar{v} \right)\,, \tag{2.13}$$

where $\bar{v} = v(\boldsymbol{x}, \overline{s})$.

In addition, equations (2.3),(2.7) and (2.9) imply that the following boundary condition is given for the function q

$$q(\boldsymbol{x}, s) = \psi(\boldsymbol{x}, s)\,, \quad \forall\ (\boldsymbol{x}, s) \in \partial\Omega \times [\underline{s}, \overline{s}]\,, \tag{2.14}$$

where

$$\psi(\boldsymbol{x}, s) = \frac{\partial}{\partial s} \left(\frac{\ln \varphi(\boldsymbol{x}, s)}{s^2} \right)\,. \tag{2.15}$$

The problem, (2.13), is nonlinear. In addition both functions q and $\bar{v}$ are unknown here. If we approximate them well, then the target coefficient $a(\boldsymbol{x})$ would be reconstructed easily via backwards calculations.

2.2 Layer Stripping with Respect to the Source Position

We now describe in detail how to discretize for s-variable. An analogue of the nonlinear equation of this section for a different CIP, in which the original PDE

was either hyperbolic or parabolic was previous derived in [15]. However there are substantial differences because [15] uses piecewise constant functions but ours use piecewise linear continuous functions.

2.2.1 Nonlinear Equation

We approximate the function $q(\boldsymbol{x}, s)$ as a *continuous piecewise linear function* with respect to the source position s. That is, we assume that there exists a partition

$$\underline{s} = s_N < s_{N-1} < \cdots < s_1 < s_0 = \overline{s}, \quad s_{n-1} - s_n = h \tag{2.16}$$

of the interval $[\underline{s}, \overline{s}]$ with sufficient small grid step size h such that

$$q(\boldsymbol{x}, s) = \frac{s_{n-1} - s}{h} q_n(\boldsymbol{x}) + \frac{s - s_n}{h} q_{n-1}(\boldsymbol{x}) \quad \text{for } s \in [s_n, s_{n-1}) \tag{2.17}$$

where $q_n(\boldsymbol{x}) = q(\boldsymbol{x}, s_n)$. We have the following approximation by the trapezoidal rule:

$$\begin{aligned} \int_s^{\overline{s}} q(\boldsymbol{x}, \tau)\, d\tau \approx{}& \frac{s_{n-1} - s}{2} \big(q_n(\boldsymbol{x}) + q_{n-1}(\boldsymbol{x})\big) \\ &+ \begin{cases} 0, & n = 1 \\ \dfrac{h}{2}\Big(q_0(\boldsymbol{x}) + 2\displaystyle\sum_{j=1}^{n-2} q_j(\boldsymbol{x}) + q_{n-1}(\boldsymbol{x})\Big), & n \geq 2 \end{cases} \end{aligned} \tag{2.18}$$

We approximate the boundary condition (2.14) as a piecewise linear continuous function,

$$\psi(\boldsymbol{x}, s) = \frac{s_{n-1} - s}{h} \psi_n(\boldsymbol{x}) + \frac{s - s_n}{h} \psi_{n-1}(\boldsymbol{x}), \text{ for } s \in [s_n, s_{n-1}) \text{ and } \boldsymbol{x} \in \partial\Omega\,, \tag{2.19}$$

where

$$\psi_n = \psi(\boldsymbol{x}, s_n)\,. \tag{2.20}$$

Introduce the new notations

$$q_n^s(\boldsymbol{x}) = \begin{cases} q_0(\boldsymbol{x}), & n = 0 \\ \dfrac{s_{n-1} - s}{h} q_n(\boldsymbol{x}) + \dfrac{s - s_n}{h} q_{n-1}(\boldsymbol{x}), & n \geq 1 \text{ and } s \in [s_n, s_{n-1}) \end{cases}, \tag{2.21}$$

$$\psi_n^s(\boldsymbol{x}) = \begin{cases} \psi_0(\boldsymbol{x}), & n = 0 \\ \dfrac{s_{n-1} - s}{h}\psi_n(\boldsymbol{x}) + \dfrac{s - s_n}{h}\psi_{n-1}(\boldsymbol{x}), & n \geq 1 \text{ and } s \in [s_n, s_{n-1}) \end{cases} \tag{2.22}$$

and

$$T_n = \left\{ \begin{array}{ll} 0, & n = 1 \\ \dfrac{h}{2}\left(q_0(\boldsymbol{x}) + 2\displaystyle\sum_{j=1}^{n-2} q_j(\boldsymbol{x}) + q_{n-1}(\boldsymbol{x}) \right), & n \geq 2 \end{array} \right\} - \bar{v}\,. \tag{2.23}$$

We substitute equations (2.17), (2.18) and (2.19) to (2.13) to obtain

– for $n = 0$

$$\Delta q_0^s \, + 2s_0^2 \nabla q_0^s \cdot \nabla \bar{v} + 4s_0 (\nabla \bar{v})^2 = -\frac{2}{s_0}(\Delta \bar{v})\,, \tag{2.24}$$

– and for $n \geq 1$

$$\begin{aligned} &\Delta q_n^s(\boldsymbol{x}) - A_n(\nabla q_n^s)^2 - B_n \nabla q_n^s \nabla q_{n-1} - C_n \nabla q_n^s \nabla T_n \\ &\quad = D_n \Delta q_{n-1}(\boldsymbol{x}) + E_n \Delta T_n - F_n(\nabla q_{n-1})^2 - G_n \nabla q_{n-1} \nabla T_n - H_n(\nabla T_n)^2 \end{aligned} \tag{2.25}$$

where

$$\begin{aligned} A_n &= (s_{n-1} - s)s^2, & B_n &= \frac{(s_{n-1} - s)(3s - 2s_{n-1})s^2}{2s - s_{n-1}}, \\ C_n &= \frac{2s^2(3s - 2s_{n-1})}{2s - s_{n-1}}, & D_n &= \frac{s_{n-1} - s}{2s - s_{n-1}}, \\ E_n &= \frac{2}{2s - s_{n-1}}, & F_n &= \frac{s^2(s_{n-1} - s)^2}{2s - s_{n-1}}, \\ G_n &= \frac{4s^2(s_{n-1} - s)}{2s - s_{n-1}}, & H_n &= \frac{4s^2}{2s - s_{n-1}}\,. \end{aligned} \tag{2.26}$$

We have

$$\max_{1 \leq n \leq N} \{|A_n|\} < h\bar{s}^2\,.$$

With the latter term, by taking h small, we mitigate the influence of the nonlinear term with $(\nabla q_n^s)^2$ in equation (2.25), and we use this in our iterative algorithm via solving a linear problem on each iterative step.

2.2.2 Reconstruction of the Target Coefficient

Suppose that functions $\{q_n\}_{n=0}^{N-1} = \{q_n^s\}_{n=0}^{N-1}$, where parameter s of q_n^s is evaluated at s_n, are approximated via solving problems (2.21), (2.22) and (2.25) and that the tail-function is also approximated. Then we construct the target coefficient $a(\boldsymbol{x})$ by backward calculation as follows. First we reconstruct the function $u_n(\boldsymbol{x}) = u(\boldsymbol{x}, s_n)$ by (2.7) as

$$u_n(\boldsymbol{x}) = \begin{cases} s_0^2 v_\infty(\boldsymbol{x}), & n = 0 \\ s_n^2 \left[-\dfrac{h}{2} \left(q_0(\boldsymbol{x}) + 2\sum_{j=1}^{n-1} q_j(\boldsymbol{x}) + q_n(\boldsymbol{x}) \right) + v_\infty(\boldsymbol{x}) \right], & n \geq 1 \end{cases}, \quad (2.27)$$

where $v_\infty(\boldsymbol{x})$ is approximation of tail-function $\bar{v}(\boldsymbol{x})$, the heuristic approach of approximating v_∞ is explained in Section 5. Hence, we first reconstruct the function $w_n(\boldsymbol{x}) = w(\boldsymbol{x}, s_n)$ as

$$w_n(\boldsymbol{x}) = \exp[u_n(\boldsymbol{x})]\,. \quad (2.28)$$

Using the Finite element method we can solve for the coefficient a(x), see [6],[7],[8] for the detail of reconstruction. We use equation (2.4) in the weak form as

$$-\int_\Omega \nabla w \nabla \eta_k d\mathbf{x} = \int_\Omega a w \eta_k d\mathbf{x}, \quad (2.29)$$

where the test function $\eta_k(\mathbf{x}), k = 1, ..., K$ is a quadratic finite element of a computational mesh with $\eta_k(\mathbf{x}) \mid_{\partial\Omega} = 0$. The number K is finite and depends on the mesh we choose. This leads to a linear algebraic system which we solve to find the function $a(\boldsymbol{x})$.

2.2.3 The Algorithm for Approximating Function q_n^s

In this subsection we describe an algorithm of sequential solutions for $n = 0, \ldots, N$ of boundary value problem (2.22) and (2.25), assuming that an approximation $v_\infty(\boldsymbol{x})$ for the tail-function is found, see Section 5. For the sake of convenience

of our analysis of our convergence theorem, we assume here and in Section 4 that our domain of interest Ω is such that its boundary $\partial\Omega \in C^{2+\alpha}$, α =const.> 0. We also assume that functions $\psi_n^s(\boldsymbol{x}) \in C^{2+\alpha}(\partial\Omega)$, $v_\infty \in C^{2+\alpha}(\partial\overline{\Omega})$. We rely on the classic Schauder theorem (§1 of Chapter 3 of [16]), which we reformulate in subsection 4.1. In addition, we assume that for each n we make infinitely many inner iterations to ensure convergence of functions $q_{n,k}^s \in C^{2+\alpha}(\overline{\Omega})$, $k \to \infty$ to function q_n^s in space $C^{2+\alpha}(\overline{\Omega})$. This convergence is established in Theorem 4.1. Since it is practically impossible to arrange infinitely many iterations, this is one of the discrepancies between our theory and computational practice.

Step 0. We need to find an approximation for the function q_0^s. To do this, we solve equation (2.24) for q_0^s with boundary condition (2.22) and use v_∞ instead of $\bar{v}$ as follows

$$\Delta q_0^s + 2s_0^2 \nabla q_0^s \cdot \nabla v_\infty + 4s_0(\nabla v_\infty)^2 = -\frac{2}{s_0}(\Delta v_\infty). \tag{2.30}$$

Before the beginning of *Step 1*, we substitute the actual $\bar{v}$ in equation (2.23) with approximation v_∞ as follows:

$$T_n = \left\{ \begin{array}{ll} 0, & n = 1 \\ \dfrac{h}{2}\left(q_0^s(\boldsymbol{x}) + 2\displaystyle\sum_{j=1}^{n-2} q_j^s(\boldsymbol{x}) + q_{n-1}^s(\boldsymbol{x}) \right), & n \geq 2 \end{array} \right\} - v_\infty .$$

Step 1. We now find an approximation for the function q_1^s. To do this, we solve equation (2.25) with the boundary condition (2.22) at $n = 1$ iteratively for q_1^s. That is, we should solve

$$\begin{aligned} &\Delta q_1^s(\boldsymbol{x}) - A_1(\nabla q_1^s)^2 - B_1 \nabla q_1^s \nabla q_0^s - C_1 \nabla q_1^s \nabla T_1 \\ &\qquad = D_1 \Delta q_0^s(\boldsymbol{x}) + E_1 \Delta T_1 - F_1(\nabla q_0^s)^2 - G_1 \nabla q_0^s \nabla T_1 - H_1(\nabla T_1)^2 . \end{aligned} \tag{2.31}$$

We solve equation (2.31) iteratively as

$$\Delta q_{1,k}^s(\boldsymbol{x}) - A_1 \nabla q_{1,k}^s \nabla q_{1,k-1}^s - B_1 \nabla q_{1,k}^s \nabla q_0^s - C_1 \nabla q_{1,k}^s \nabla T_1$$

$$= D_1\Delta q_0^s(\boldsymbol{x}) + E_1\Delta T_1 - F_1(\nabla q_0^s)^2 - G_1\nabla q_0^s\,\nabla T_1 - H_1(\nabla T_1)^2 \qquad (2.32)$$

with $q_{1,k}^s(\boldsymbol{x})$ having the same boundary conditions as $q_1^s(\boldsymbol{x})$ and $q_{1,0}^s = q_0^s$.

We proceed with calculating the function $q_{1,k+1}^s$ in (2.32). We iterate in (2.32) until the process converges, i.e., $\|q_{1,k}^s - q_{1,k-1}^s\|_{L_2(\Omega)} < \epsilon$ for some $\epsilon > 0$. We set $q_1^s := q_{1,k}^s$.

Step n. We now find an approximation for the function q_n^s assuming that function $q_0^s, \ldots, q_{n-1}^s$ with respect to $s_0, \ldots, s_{n-1}$, respectively, are found. We solve iteratively equation (2.25) with the boundary condition (2.22) at arbitrary $n > 1$ as following

$$\Delta q_{n,k}^s(\boldsymbol{x}) - A_n\nabla q_{n,k}^s\nabla q_{n,k-1}^s - B_n\nabla q_{n,k}^s\nabla q_{n-1}^s - C_n\nabla q_{n,k}^s\nabla T_n$$

$$= D_n\Delta q_{n-1}^s(\boldsymbol{x}) + E_n\Delta T_n - F_n(\nabla q_{n-1}^s)^2 - G_n\nabla q_{n-1}^s\nabla T_n - H_n(\nabla T_n)^2 \qquad (2.33)$$

with $q_{n,k}^s(\boldsymbol{x})$ having the same boundary conditions as $q_n^s(\boldsymbol{x})$ and $q_{n,0}^s = q_{n-1}^s$. We iterate until the process converges, i.e., until $\|q_{n,k}^s - q_{n,k-1}^s\|_{L_2(\Omega)} < \epsilon$ for some $\epsilon > 0$. We set $q_n^s = q_{n,k}^s$.

2.3 Exact Solution of the Steady-State Problem

Following the Tikhonov concept, we need to introduce the definitions of the exact solution first. We assume that for inverse problems there exists an exact coefficient function $a^*(\boldsymbol{x}) \in C^\alpha(\overline{\Omega})$, where constant $\alpha \in (0,1)$, which is a solution of our Inverse Problem. Let the function

$$w^*(\boldsymbol{x}, s) \in C^{2+\alpha}(|\boldsymbol{x} - \boldsymbol{x}_0| \geq \varepsilon)\,,\ \forall\,\varepsilon > 0\,,\ \forall\,\boldsymbol{x}_0 = (B, s) > 0\,, \forall\, s \in [\underline{s}, \overline{s}]$$

be the solution of the problem (2.1) and (2.2) with $a(\boldsymbol{x}) := a^*(\boldsymbol{x})$. Let

$$u^*(\boldsymbol{x}, s) = \ln w^*(\boldsymbol{x}, s)\,,\ q^*(\boldsymbol{x}, s) = \frac{\partial u^*(\boldsymbol{x}, s)}{\partial s}\,,\ u_\infty^*(\boldsymbol{x}) = u^*(\boldsymbol{x}, \overline{s})\,.$$

By equation (2.5)

$$\Delta u^*(\boldsymbol{x},s)+[\nabla u^*(\boldsymbol{x},s)]^2=a^*(\boldsymbol{x})\,. \tag{2.34}$$

Also, the function q^* satisfies the following analogue of equation (2.13)

$$\Delta q^*-2s^2\nabla q^*\cdot\left(\int_s^{\overline{s}}\nabla q^*\,d\tau+\nabla\bar{v}^*\right)+4s\left(\int_s^{\overline{s}}\nabla q^*\,d\tau-\nabla\bar{v}^*\right)^2$$
$$=\frac{2}{s}\left(\int_s^{\overline{s}}\Delta q^*\,d\tau-\Delta\bar{v}^*\right) \tag{2.35}$$

with the boundary condition (2.14)

$$q^*(\boldsymbol{x},s)=\psi^*(\boldsymbol{x},s)\,,\quad \forall\ (\boldsymbol{x},s)\in\partial\Omega\times[\underline{s},\overline{s}]\,, \tag{2.36}$$

where $\psi^*(\boldsymbol{x},s)=\frac{\partial}{\partial s}\ln\varphi^*(\boldsymbol{x},s)$, where $\varphi^*(\boldsymbol{x},s)=w^*(\boldsymbol{x},s)$ for $(\boldsymbol{x},s)\in\partial\Omega\times[\underline{s},\overline{s}]$.

Definition. We call the function $q^*(\boldsymbol{x},s)$ the *exact solution* of the problem (2.13) and (2.14) with the *exact boundary* condition $\psi^*(\boldsymbol{x},s)$. Naturally, the function $a^*(\boldsymbol{x})$ from equation (2.34) is called the exact solution of our Inverse Problem.

Therefore

$$q^*(\boldsymbol{x},s)\in C^{2+\alpha}(\overline{\Omega})\times C^1[\underline{s},\overline{s}]\,. \tag{2.37}$$

We now approximate the function $q_n^*(\boldsymbol{x})$, $n\geq 0$, for representing the function $q^*(\boldsymbol{x},s)$ as follows

– for $n=0$

$$q_0^*(\boldsymbol{x})=q^*(\boldsymbol{x},s_0)$$

– and for $n\geq 1$, for any $s\in[s_n,s_{n-1})$ by averaging

$$q_n^*(\boldsymbol{x})=\frac{1}{h}\int_{s_n}^{s_{n-1}}q^*(\boldsymbol{x},s)\,ds\,,\quad \psi_n^*(\boldsymbol{x})=\frac{1}{h}\int_{s_n}^{s_{n-1}}\psi^*(\boldsymbol{x},s)\,ds$$

Then by (2.37) for $n\geq 1$

$$q^*(\boldsymbol{x},s)=q_n^*(\boldsymbol{x})+Q_n(\boldsymbol{x},s)\ ,\qquad \psi^*(\boldsymbol{x},s)=\psi_n^*(\boldsymbol{x})+\Psi_n(\boldsymbol{x},s) \tag{2.38}$$

$s \in [s_n, s_{n-1})$, where functions Q_n, Ψ_n are such that for $s \in [s_n, s_{n-1})$

$$\|Q_n(\boldsymbol{x}, s)\|_{C^{2+\alpha}(\overline{\Omega})} \leq C^* h\,,\ \|\Psi_n(\boldsymbol{x}, s)\|_{C^{2+\alpha}(\overline{\Omega})} \leq C^* h\,,$$

$$\forall\, s \in [s_n, s_{n-1})\,,\ n = 1, \ldots, N\,, \tag{2.39}$$

where the constant $C^* > 0$ depends only on $C^{2+\alpha}(\overline{\Omega}) \times C^1[\underline{s}, \overline{s}]$ and $C^{2+\alpha}(\overline{\Omega}) \times C^1[\underline{s}, \overline{s}]$ norms of function q^* and ψ^* respectively. Hence

$$q_n^*(\boldsymbol{x}) = \psi_n^*(\boldsymbol{x})\,, \quad \boldsymbol{x} \in \partial\Omega\,, \tag{2.40}$$

and the following analog of equations (2.30) and (2.33) hold

$$\Delta q_0^* + 2s_0^2 \nabla q_0^* \cdot \nabla \bar{v}^* + 4s_0 (\nabla \bar{v}^*)^2 = -\frac{2}{s_0}(\Delta \bar{v}^*) \tag{2.41}$$

and

$$\Delta q_n^*(\boldsymbol{x}) - A_n(\nabla q_n^*)^2 - B_n \nabla q_n^* \nabla q_{n-1}^* - C_n \nabla q_n^* \nabla T_n^*$$

$$= D_n \Delta q_0^*(\boldsymbol{x}) + E_n \Delta T_n^* - F_n(\nabla q_0^*)^2 - G_n \nabla q_0^* \nabla T_n^* - H_n(\nabla T_n^*)^2 + R_n(\boldsymbol{x}, h) \tag{2.42}$$

with

$$T_n^* = \left\{ \begin{array}{ll} 0, & n = 1 \\ \dfrac{h}{2}\left(q_0^*(\boldsymbol{x}) + 2\displaystyle\sum_{j=1}^{n-2} q_j^*(\boldsymbol{x}) + q_{n-1}^*(\boldsymbol{x}) \right), & n \geq 2 \end{array} \right\} - \bar{v}^*\,,$$

respectively, where the function $R_n(\boldsymbol{x}, h) \in C^\alpha(\overline{\Omega})$ and

$$\max_{1 \leq n \leq N} \|R_n(\boldsymbol{x}, h)\|_{C^{2+\alpha}(\overline{\Omega})} \leq C^* h \quad ,\ n = 1, 2, \ldots, N. \tag{2.43}$$

We also assume that the data $\varphi(\boldsymbol{x}, s)$ in (2.3) are given with error. This naturally produces an error in the function $\psi(\boldsymbol{x}, s)$ in (2.14). An additional error is introduced due to taking the average value of $\psi^*(\boldsymbol{x}, s)$ over the interval $[s_n, s_{n+1})$. Hence, it is reasonable to assume that

$$\|\psi_n^*(\boldsymbol{x}) - \psi_n^{\mathrm{s}}(\boldsymbol{x})\|_{C^{2+\alpha}(\partial\Omega)} \leq C_1(\sigma + h)\,, \tag{2.44}$$

where $\sigma > 0$ is a small parameter characterizing the level of the error in the data $\varphi(\boldsymbol{x}, s)$ and the constant $C_1 > 0$ is independent on numbers σ, h and n.

CHAPTER 3

MATHEMATICAL MODEL FOR THE TIME-DEPENDENT PROBLEM

Now we examine equation (1.1) which depends on $\boldsymbol{x}$ and t with the following inverse problem:

$$-w_t(\boldsymbol{x},t) + \Delta w(\boldsymbol{x},t) - a(\boldsymbol{x})w(\boldsymbol{x},t) = 0$$

where $w(\boldsymbol{x},0) = \delta(\boldsymbol{x}-\boldsymbol{x}_0)$,

$$\lim_{|\boldsymbol{x}|\to\infty} w(\boldsymbol{x},t) = 0\,.$$

The Inverse Problem

Denote $\boldsymbol{x} = (x,y)$. Let $\Omega \subset \mathbb{R}^2$ be a bounded domain and $\Gamma = \partial\Omega$. Determine the coefficient $a(\boldsymbol{x})$ in equation (1.1) for $\boldsymbol{x} \in \Omega$, assuming that the following function $\varphi(\boldsymbol{x},t)$ is given

$$w(\boldsymbol{x},t) = \varphi(\boldsymbol{x},t), \qquad \forall \boldsymbol{x} \in \Gamma, \quad \forall t \in [0,T], \tag{3.1}$$

We show above in Fig. (3.1) the geometry for the inverse problem.

3.1 Nonlinear Integral Differential Equation

We perform $L(u) = \int_0^\infty e^{-s^2t} w(\boldsymbol{x},t)dt, s > 0$ a Laplace-like Transform on Eq. (1.1) .

$$-\int_0^\infty e^{-s^2t} w_t dt + \Delta \int_0^\infty e^{-s^2t} w dt - a(\boldsymbol{x}) \int_0^\infty e^{-s^2t} w dt = 0 \tag{3.2}$$

and use Integration by Parts to get

$$-s^2 \int_0^\infty e^{-s^2t} w dt + \Delta \int_0^\infty e^{-s^2t} w dt - a(\boldsymbol{x}) \int_0^\infty e^{-s^2t} w dt = -\delta(\boldsymbol{x}-\boldsymbol{x}_0) \tag{3.3}$$

Let

$$\tilde{u} = \int_0^\infty e^{-s^2t} w(\boldsymbol{x},t)dt \tag{3.4}$$

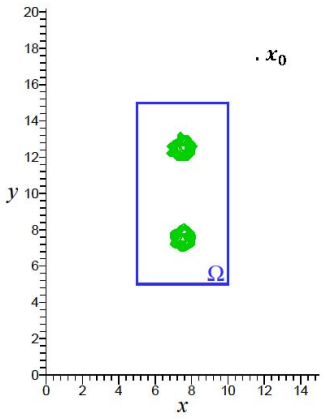

Figure 3.1. The geometry of the time-dependent inverse problem, . .

and we arrive at a similar equation to the steady-state optical tomography problem.

$$\Delta\tilde{u}(\boldsymbol{x}, s) - (a(\boldsymbol{x}) + s^2)\tilde{u}(\boldsymbol{x}, s) = -\delta(\boldsymbol{x} - \boldsymbol{x}_0) \tag{3.5}$$

Function w is positive by the maximum principle, we can consider the function $u = \ln \tilde{u}$ and obtain the following equation from equation (3.5) with the light source term removed for $\boldsymbol{x} \in \Omega$

$$\Delta u(\boldsymbol{x}, s) + [\nabla u(\boldsymbol{x}, s)]^2 = a(\boldsymbol{x}) + s^2 \quad \boldsymbol{x} \in \Omega \tag{3.6}$$

$$u(\boldsymbol{x}, s) = \phi(\boldsymbol{x}, s) \quad \forall\ (\boldsymbol{x}, s) \in \Gamma \times (\underline{s}, \overline{s})\,, \tag{3.7}$$

where $\phi = \ln \varphi$.

We deduce another form of the inverse problem as follows: Let

$$v(\boldsymbol{x}, s) = \frac{u(\boldsymbol{x}, s)}{s^2}\,. \tag{3.8}$$

Equation (3.6) becomes

$$\Delta v(\boldsymbol{x}, s) + s^2[\nabla v(\boldsymbol{x}, s)]^2 = \frac{a(\boldsymbol{x})}{s^2} + 1 \tag{3.9}$$

Denote

$$q(\boldsymbol{x}, s) = \frac{\partial}{\partial s} v(\boldsymbol{x}, s)\,. \tag{3.10}$$

We have

$$\Delta q(\boldsymbol{x},s)+2s^2\nabla q(\boldsymbol{x},s)\cdot\nabla v(\boldsymbol{x},s)+2s[\nabla v(\boldsymbol{x},s)]^2=-2\frac{a(\boldsymbol{x})}{s^3}\,, \tag{3.11}$$

$$\boldsymbol{x}\in\Omega\,,\quad s\in(\underline{s},\overline{s}]$$

where

$$v(\boldsymbol{x},s)=-\int_s^{\overline{s}}q(\boldsymbol{x},\tau)\,d\tau+v(\boldsymbol{x},\overline{s})\,,\quad \boldsymbol{x}\in\Omega\,,\quad s\in[\underline{s},\overline{s}] \tag{3.12}$$

where $\overline{s}$ is a large number which will be chosen in numerical experiments. The new small tail-function in equation (3.12) is obtained by

$$v(\boldsymbol{x},\overline{s})=\frac{u(\boldsymbol{x},\overline{s})}{\overline{s}^2}\,. \tag{3.13}$$

We obtain from eq. (3.9), (3.11) and (3.12) the following "Nonlinear Integral Differential Equation"

$$\Delta q+2s^2\nabla q\cdot\left(-\int_s^{\overline{s}}\nabla q\,d\tau+\nabla\bar{v}\right)+4s\left(-\int_s^{\overline{s}}\nabla q\,d\tau+\nabla\bar{v}\right)^2$$
$$=-\frac{2}{s}\left(-\int_s^{\overline{s}}\Delta q\,d\tau+\Delta\bar{v}\right)+\frac{2}{s}\,, \tag{3.14}$$

where $\bar{v}=v(\boldsymbol{x},\overline{s})$.

In addition, equations (3.1),(3.8) and (3.10) imply that the following boundary condition is given for the function q

$$q(\boldsymbol{x},s)=\psi(\boldsymbol{x},s)\,,\quad\forall\ (\boldsymbol{x},s)\in\partial\Omega\times[\underline{s},\overline{s}]\,, \tag{3.15}$$

where

$$\psi(\boldsymbol{x},s)=\frac{\partial}{\partial s}\left(\frac{\ln\varphi(\boldsymbol{x},s)}{s^2}\right)\,. \tag{3.16}$$

The problem (3.14-3.15) is nonlinear. In addition both functions q and $\bar{v}$ are unknown here. If we approximate them well (in a certain sense, specified below), then the target coefficient $a(\boldsymbol{x})$ would be reconstructed via backwards calculations.

3.2 Layer Stripping with Respect to the Frequency

We now describe in detail how to discretize for s-variable. An analogue of the nonlinear equation of this section for a different CIP, in which the governing PDE was either hyperbolic or parabolic was previous derived in [15]. However there are substantial differences because [15] uses a piecewise constant function but ours uses optical piecewise linear continuous functions. The goal in [15] was to seek optical scattering coefficients, but in this problem the absorption is sought.

3.2.1 Nonlinear Equation

We approximate the function $q(\boldsymbol{x}, s)$ as a *continuous piecewise linear function* with respect to the pseudo frequency s. That is, we assume that there exists a partition

$$\underline{s} = s_N < s_{N-1} < \cdots < s_1 < s_0 = \overline{s}, \quad s_{n-1} - s_n = h \tag{3.17}$$

of the interval $[\underline{s}, \overline{s}]$ with sufficient small grid step size h such that

$$q(\boldsymbol{x}, s) = \frac{s_{n-1} - s}{h} q_n(\boldsymbol{x}) + \frac{s - s_n}{h} q_{n-1}(\boldsymbol{x}) \quad \text{for } s \in [s_n, s_{n-1}) \tag{3.18}$$

where $q_n(\boldsymbol{x}) = q(\boldsymbol{x}, s_n)$. We have following approximation by trapezoidal rule:

$$\int_s^{\overline{s}} q(\boldsymbol{x}, \tau)\, d\tau \approx \frac{s_{n-1} - s}{2} \big(q_n(\boldsymbol{x}) + q_{n-1}(\boldsymbol{x})\big) + \begin{cases} 0, & n = 1 \\ \dfrac{h}{2}\Big(q_0(\boldsymbol{x}) + 2\displaystyle\sum_{j=1}^{n-2} q_j(\boldsymbol{x}) + q_{n-1}(\boldsymbol{x})\Big), & n \geq 2 \end{cases}. \tag{3.19}$$

We approximate the boundary condition (3.15) as a piecewise linear continuous function,

$$\psi(\boldsymbol{x}, s) = \frac{s_{n-1} - s}{h} \psi_n(\boldsymbol{x}) + \frac{s - s_n}{h} \psi_{n-1}(\boldsymbol{x}), \text{ for } s \in [s_n, s_{n-1}) \text{ and } \boldsymbol{x} \in \partial\Omega\,, \tag{3.20}$$

where

$$\psi_n = \psi(\boldsymbol{x}, s_n)\,. \tag{3.21}$$

Introduce the new notations

$$q_n^s(\boldsymbol{x}) = \begin{cases} q_0(\boldsymbol{x}), & n = 0 \\ \dfrac{s_{n-1} - s}{h} q_n(\boldsymbol{x}) + \dfrac{s - s_n}{h} q_{n-1}(\boldsymbol{x}), & n \geq 1 \text{ and } s \in [s_n, s_{n-1}) \end{cases}, \tag{3.22}$$

$$\psi_n^s(\boldsymbol{x}) = \begin{cases} \psi_0(\boldsymbol{x}), & n = 0 \\ \dfrac{s_{n-1} - s}{h} \psi_n(\boldsymbol{x}) + \dfrac{s - s_n}{h} \psi_{n-1}(\boldsymbol{x}), & n \geq 1 \text{ and } s \in [s_n, s_{n-1}) \end{cases} \tag{3.23}$$

and

$$T_n = \left\{ \begin{array}{ll} 0, & n = 1 \\ \dfrac{h}{2} \left(q_0(\boldsymbol{x}) + 2 \displaystyle\sum_{j=1}^{n-2} q_j(\boldsymbol{x}) + q_{n-1}(\boldsymbol{x}) \right), & n \geq 2 \end{array} \right\} - \bar{v}\,. \tag{3.24}$$

We substitute equations (3.18), (3.19) and (3.20) to (3.14) to obtain

– for $n = 0$

$$\Delta q_0^s \, + 2 s_0^2 \nabla q_0^s \cdot \nabla \bar{v} + 4 s_0 (\nabla \bar{v})^2 = -\frac{2}{s_0} (\Delta \bar{v}) + \frac{2}{s_0}\,, \tag{3.25}$$

– and for $n \geq 1$

$$\begin{aligned} &\Delta q_n^s(\boldsymbol{x}) - A_n (\nabla q_n^s)^2 - B_n \nabla q_n^s \nabla q_{n-1} - C_n \nabla q_n^s \nabla T_n \\ &\quad = D_n \Delta q_{n-1}(\boldsymbol{x}) + E_n \Delta T_n - F_n (\nabla q_{n-1})^2 - G_n \nabla q_{n-1} \nabla T_n - H_n (\nabla T_n)^2 + \frac{2}{s_n} \end{aligned} \tag{3.26}$$

where

$$\begin{aligned} A_n &= (s_{n-1}-s)s^2, & B_n &= \frac{(s_{n-1}-s)(3s-2s_{n-1})s^2}{2s-s_{n-1}}, \\ C_n &= \frac{2s^2(3s-2s_{n-1})}{2s-s_{n-1}}, & D_n &= \frac{s_{n-1}-s}{2s-s_{n-1}}, \\ E_n &= \frac{2}{2s-s_{n-1}}, & F_n &= \frac{s^2(s_{n-1}-s)^2}{2s-s_{n-1}}, \\ G_n &= \frac{4s^2(s_{n-1}-s)}{2s-s_{n-1}}, & H_n &= \frac{4s^2}{2s-s_{n-1}}. \end{aligned} \tag{3.27}$$

We have

$$\max_{1\le n\le N}\{|A_n|\} < h\overline{s}^2 .$$

With the latter term, by taking h small, we mitigate the influence of the nonlinear term with $(\nabla q_n^s)^2$ in equation (3.26), and we use this in our iterative algorithm via solving a linear problem on each iterative step.

3.2.2 Reconstruction of the Target Coefficient

Suppose that functions $\{q_n\}_{n=0}^{N-1} = \{q_n^s\}_{n=0}^{N-1}$, where parameter s of q_n^s is evaluated at s_n, are approximated via solving problems (3.22), (3.23) and (3.26) and that the tail-function is also approximated. Then we construct the target coefficient $a(\boldsymbol{x})$ by backward calculation as follows. First we reconstruct the function $u_n(\boldsymbol{x}) = u(\boldsymbol{x}, s_n)$ by (3.8) as

$$u_n(\boldsymbol{x}) = \begin{cases} s_0^2 v_\infty(\boldsymbol{x}), & n = 0 \\ s_n^2\left[-\dfrac{h}{2}\left(q_0(\boldsymbol{x}) + 2\displaystyle\sum_{j=1}^{n-1} q_j(\boldsymbol{x}) + q_n(\boldsymbol{x})\right) + v_\infty(\boldsymbol{x})\right], & n \ge 1 \end{cases}, \tag{3.28}$$

where $v_\infty(\boldsymbol{x})$ is an approximation of the tail-function $\bar{v}(\boldsymbol{x})$, the heuristic approach of approximating v_∞ is explained in section (6). Hence, we first reconstruct the function $\tilde{u}_n(\boldsymbol{x}) = \tilde{u}(\boldsymbol{x}, s_n)$ as

$$\tilde{u}_n(\boldsymbol{x}) = \exp[u_n(\boldsymbol{x})]\,. \tag{3.29}$$

Using the Finite Element Method we can solve for the coefficient $a(x)$ see [6],[7],[8] for the details of the reconstruction. We use equation (3.5) in the weak form as

$$-\int_\Omega \nabla\tilde{u}\nabla\eta_k d\mathbf{x} + \int_\Omega \delta\eta_k d\mathbf{x} = \int_\Omega (a+s^2)\tilde{u}\eta_k d\mathbf{x}, \tag{3.30}$$

where the test function $\eta_k(\mathbf{x}), k = 1, ..., K$ is a quadratic finite element of a computational mesh with $\eta_k(\mathbf{x})\,|_{\partial\Omega} = 0$. The number K is finite and depends on the mesh we choose. This leads to a linear algebraic system which we solve to find the function $a(\boldsymbol{x})$.

3.2.3 The Algorithm for Approximating Function q_n^s

In this subsection we describe an algorithm of sequential solutions for $n = 0, \ldots, N$ of boundary value problem (3.23) and (3.26), assuming that an approximation $v_\infty(\boldsymbol{x})$ for the tail-function is found, see Section 6. For the sake of convenience of our convergence analysis, we assume here and in Section 4 that our domain of interest Ω is such that its boundary $\partial\Omega \in C^{2+\alpha}$, α =const.> 0. We also assume that functions $\psi_n^s(\boldsymbol{x}) \in C^{2+\alpha}(\partial\Omega)$, $v_\infty \in C^{2+\alpha}(\partial\overline{\Omega})$. We rely on the classic Schauder theorem (§1 of Chapter 3 of [16]), which we reformulate in subsection 4.1. In addition, we assume that for each n we make infinitely many inner iterations to ensure convergence of functions $q_{n,k}^s \in C^{2+\alpha}(\overline{\Omega})$, $k \to \infty$ to function q_n^s in space $C^{2+\alpha}(\overline{\Omega})$. This convergence is established in Theorem 4.1.

Step 0. We need to find an approximation for the function q_0^s. To do this, we solve equation (3.25) for q_0^s with boundary condition (3.23) and use the approximation v_∞ instead of $\bar{v}$ as follows

$$\Delta q_0^s + 2s_0^2 \nabla q_0^s \cdot \nabla v_\infty + 4s_0(\nabla v_\infty)^2 = -\frac{2}{s_0}(\Delta v_\infty) + \frac{2}{s} \tag{3.31}$$

Before beginning of *Step 1*, we substitute the actual $\bar{v}$ in equation (3.24) with the approximation v_∞ as follows:

$$T_n = \left\{ \begin{array}{ll} 0, & n = 1 \\ \dfrac{h}{2}\left(q_0^s(\boldsymbol{x}) + 2\displaystyle\sum_{j=1}^{n-2} q_j^s(\boldsymbol{x}) + q_{n-1}^s(\boldsymbol{x}) \right), & n \geq 2 \end{array} \right\} - v_\infty .$$

Step 1. We now find an approximation for the function q_1^s. To do this, we solve equation (3.26) with the boundary condition (3.23) at $n = 1$ iteratively for q_1^s. That is, we should solve

$$\begin{aligned} &\Delta q_1^s - A_1(\nabla q_1^s)^2 - B_1 \nabla q_1^s \nabla q_0^s - C_1 \nabla q_1^s \nabla T_1 \\ &\qquad = D_1 \Delta q_0^s + E_1 \Delta T_1 - F_1(\nabla q_0^s)^2 - G_1 \nabla q_0^s \nabla T_1 - H_1(\nabla T_1)^2 + \frac{2}{s_1} . \end{aligned} \tag{3.32}$$

We solve equation (3.32) iteratively as

$$\begin{aligned} &\Delta q_{1,k}^s - A_1 \nabla q_{1,k}^s \nabla q_{1,k-1}^s - B_1 \nabla q_{1,k}^s \nabla q_0^s - C_1 \nabla q_{1,k}^s \nabla T_1 \\ &\qquad = D_1 \Delta q_0^s + E_1 \Delta T_1 - F_1(\nabla q_0^s)^2 - G_1 \nabla q_0^s \nabla T_1 - H_1(\nabla T_1)^2 + \frac{2}{s_1} \end{aligned} \tag{3.33}$$

with $q_{1,k}^s = q_{1,k}^s(\boldsymbol{x})$ having the same boundary conditions as $q_1^s(\boldsymbol{x})$ and $q_{1,0}^s = q_0^s$.

We proceed with calculating the function $q_{1,k+1}^s$ as in (3.33). We iterate in (3.33) until the process converges, i.e., $\|q_{1,k}^s - q_{1,k-1}^s\|_{L_2(\Omega)} < \epsilon$ for some $\epsilon > 0$. We set $q_1^s := q_{1,k}^s$.

Step n. We now find an approximation for the function q_n^s assuming that function $q_0^s, \ldots, q_{n-1}^s$ with respect to $s_0, \ldots, s_{n-1}$, respectively, are found. We solve

iteratively equation (3.26) with the boundary condition (3.23) at arbitrary $n > 1$ as following

$$\Delta q^s_{n,k} - A_n \nabla q^s_{n,k} \nabla q^s_{n,k-1} - B_n \nabla q^s_{n,k} \nabla q^s_{n-1} - C_n \nabla q^s_{n,k} \nabla T_n$$

$$= D_n \Delta q^s_{n-1} + E_n \Delta T_n - F_n (\nabla q^s_{n-1})^2 - G_n \nabla q^s_{n-1} \nabla T_n - H_n (\nabla T_n)^2 + \frac{2}{s_n} \quad (3.34)$$

with $q^s_{n,k} = q^s_{n,k}(\boldsymbol{x})$ having the same boundary conditions as $q^s_n(\boldsymbol{x})$ and $q^s_{n,0} = q^s_{n-1}$. We iterate until the precess converges, i.e., until $\|q^s_{n,k} - q^s_{n,k-1}\|_{L_2(\Omega)} < \epsilon$ for some $\epsilon > 0$. We set $q^s_n = q^s_{n,k}$.

3.3 Exact Solution of the Time-Dependent Problem

Following the Tikhonov concept, we need to introduce the definitions of the exact solution first. We assume that there exists an exact coefficient function $a^*(\boldsymbol{x}) \in C^\alpha(\overline{\Omega})$, where constant $\alpha \in (0,1)$, which is a solution of our Inverse Problem. Let the function

$$\tilde{u}^*(\boldsymbol{x}, s) \in C^{2+\alpha}(|\boldsymbol{x} - \boldsymbol{x}_0| \geq \varepsilon)\,,\ \forall\, \varepsilon > 0\,,\ \forall\, \boldsymbol{x}_0 > 0\,, \forall\, s \in [\underline{s}, \overline{s}]$$

be the solution of the Laplace Transform of problem (1.1), (1.2) with $a(\boldsymbol{x}) := a^*(\boldsymbol{x})$. Let

$$u^*(\boldsymbol{x}, s) = \ln \tilde{u}^*(\boldsymbol{x}, s)\,,\ q^*(\boldsymbol{x}, s) = \frac{\partial u^*(\boldsymbol{x}, s)}{\partial s}\,,\ u^*_\infty(\boldsymbol{x}) = u^*(\boldsymbol{x}, \overline{s})\,.$$

By standard Holder estimate, we have

$$q^*(\boldsymbol{x}, s) \in C^{2+\alpha}(\overline{\Omega}) \times C^1[\underline{s}, \overline{s}]\,. \quad (3.35)$$

By equation (3.6) we get

$$\Delta u^*(\boldsymbol{x}, s) + [\nabla u^*(\boldsymbol{x}, s)]^2 = a^*(\boldsymbol{x}) + s^2\,. \quad (3.36)$$

Also, the function q^* satisfies the following analogue of equation (3.14)

$$\Delta q^* - 2s^2 \nabla q^* \cdot \left(\int_s^{\overline{s}} \nabla q^* \, d\tau + \nabla \bar{v}^* \right) + 4s \left(\int_s^{\overline{s}} \nabla q^* \, d\tau - \nabla \bar{v}^* \right)^2$$

$$= \frac{2}{s} \left(\int_s^{\overline{s}} \Delta q^* \, d\tau - \Delta \bar{v}^* \right) + \frac{2}{s} \tag{3.37}$$

with the boundary condition (3.15)

$$q^*(\boldsymbol{x}, s) = \psi^*(\boldsymbol{x}, s) \,, \quad \forall \, (\boldsymbol{x}, s) \in \partial\Omega \times [\underline{s}, \overline{s}] \,, \tag{3.38}$$

where $\psi^*(\boldsymbol{x}, s) = \frac{\partial}{\partial s} \ln \varphi^*(\boldsymbol{x}, s)$, where $\varphi^*(\boldsymbol{x}, s) = \tilde{u}^*(\boldsymbol{x}, s)$ for $(\boldsymbol{x}, s) \in \partial\Omega \times [\underline{s}, \overline{s}]$.

Definition. We call the function $q^*(\boldsymbol{x}, s)$ the *exact solution* of the problem (3.14), (3.15) with the *exact boundary* condition $\psi^*(\boldsymbol{x}, s)$. Naturally, the function $a^*(\boldsymbol{x})$ from equation (3.36) is called the exact solution of our Inverse Problem.

We now approximate the function $q_n^*(\boldsymbol{x})$, $n \geq 0$, for representing the function $q^*(\boldsymbol{x}, s)$ as follows

– for $n = 0$

$$q_0^*(\boldsymbol{x}) = q^*(\boldsymbol{x}, s_0)$$

– and for $n \geq 1$, for any $s \in [s_n, s_{n-1})$ by averaging

$$q_n^*(\boldsymbol{x}) = \frac{1}{h} \int_{s_n}^{s_{n-1}} q^*(\boldsymbol{x}, s) \, ds \,, \quad \psi_n^*(\boldsymbol{x}) = \frac{1}{h} \int_{s_n}^{s_{n-1}} \psi^*(\boldsymbol{x}, s) \, ds.$$

Then by (3.35) for $n \geq 1$

$$q^*(\boldsymbol{x}, s) = q_n^*(\boldsymbol{x}) + Q_n(\boldsymbol{x}, s) \,, \qquad \psi^*(\boldsymbol{x}, s) = \psi_n^*(\boldsymbol{x}) + \Psi_n(\boldsymbol{x}, s), \tag{3.39}$$

$s \in [s_n, s_{n-1})$, where functions Q_n, Ψ_n are such that for $s \in [s_n, s_{n-1})$

$$\| Q_n(\boldsymbol{x}, s) \|_{C^{2+\alpha}(\overline{\Omega})} \leq C^* h \,, \; \| \Psi_n(\boldsymbol{x}, s) \|_{C^{2+\alpha}(\overline{\Omega})} \leq C^* h \,,$$

$$\forall \, s \in [s_n, s_{n-1}) \,, \; n = 1, \ldots, N \,, \tag{3.40}$$

where the constant $C^* > 0$ depends only on $C^{2+\alpha}(\overline{\Omega}) \times C^1[\underline{s}, \overline{s}]$ and $C^{2+\alpha}(\overline{\Omega}) \times C^1[\underline{s}, \overline{s}]$ norms of function q^* and ψ^* respectively. Hence

$$q_n^*(\boldsymbol{x}) = \psi_n^*(\boldsymbol{x}), \quad \boldsymbol{x} \in \partial\Omega, \tag{3.41}$$

and the following analog of equations (3.31) and (3.34) hold

$$\Delta q_0^* + 2s_0^2 \nabla q_0^* \cdot \nabla \bar{v}^* + 4s_0 (\nabla \bar{v}^*)^2 = -\frac{2}{s_0}(\Delta \bar{v}^*) + \frac{2}{s_0} \tag{3.42}$$

and

$$\Delta q_n^*(\boldsymbol{x}) - A_n(\nabla q_n^*)^2 - B_n \nabla q_n^* \nabla q_{n-1}^* - C_n \nabla q_n^* \nabla T_n^*$$

$$= D_n \Delta q_0^*(\boldsymbol{x}) + E_n \Delta T_n^* - F_n(\nabla q_0^*)^2 - G_n \nabla q_0^* \nabla T_n^* - H_n(\nabla T_n^*)^2 + \frac{2}{s_n} + R_n(\boldsymbol{x}, h) \tag{3.43}$$

with

$$T_n^* = \left\{ \begin{array}{ll} 0, & n = 1 \\ \dfrac{h}{2}\left(q_0^*(\boldsymbol{x}) + 2\displaystyle\sum_{j=1}^{n-2} q_j^*(\boldsymbol{x}) + q_{n-1}^*(\boldsymbol{x}) \right), & n \geq 2 \end{array} \right\} - \bar{v}^*,$$

respectively, where the function $R_n(\boldsymbol{x}, h) \in C^\alpha(\overline{\Omega})$ and

$$\max_{1 \leq n \leq N} \|R_n(\boldsymbol{x}, h)\|_{C^{2+\alpha}(\overline{\Omega})} \leq C^* h \quad , \ n = 1, 2, \ldots, N. \tag{3.44}$$

We also assume that the data $\varphi(\boldsymbol{x}, s)$ in (3.1) are given with error. This naturally produces an error in the function $\psi(\boldsymbol{x}, s)$ in (3.15). An additional error is introduced due to taking the average value of $\psi^*(\boldsymbol{x}, s)$ over the interval $[s_n, s_{n+1})$. Hence, it is reasonable to assume that

$$\|\psi_n^*(\boldsymbol{x}) - \psi_n^s(\boldsymbol{x})\|_{C^{2+\alpha}(\partial\Omega)} \leq C_1(\sigma + h), \tag{3.45}$$

where $\sigma > 0$ is a small parameter characterizing the level of the error in the data $\varphi(\boldsymbol{x}, s)$ and the constant $C_1 > 0$ is independent on numbers σ, h and n.

CHAPTER 4

CONVERGENCE OF THE INVERSE PROBLEM

Below we follow the concept of Tikhonov for ill-posed problems [17], which is one of the backbones of this theory. By this concept one should assume first that there exists an "ideal" exact solution of the problem with the exact data. Next, one should assume the presence of an error in the data of the level ζ, where $\zeta > 0$ is a small parameter. Suppose that an approximate solution is constructed for a sufficiently small ζ. This solution is called a "regularized solution", if the ζ-dependent family of these solutions tends to that exact solution as ζ tends to zero. Hence, one should prove this convergence (Theorem 4.1).

In this section we use the Schauder's theorem [16] to estimate function $q^s_{n,k}$. Since the Schauder's theorem requires $C^{2+\alpha}$ smoothness of the boundary $\partial\Omega$, we assume in this section that $\Omega \in \mathbb{R}^2$ is a convex bounded domain with $\partial\Omega \in C^{2+\alpha}$. This is in a disagreement with our domain Ω in numerical experiments that is rectangle. However we use the rectangle only because of the problem of the tail-function, in which we cannot approximate it well heuristically for the case of a more general domain. However, an analogue of our convergence result (Theorem 4.1) can be proven for the case when Ω is rectangle and an FEM (i.e. discrete) version of equation (2.24), (2.25), or (3.25), (3.26) depending on the problem is considered with a fixed number R of finite elements. To do this, one need to consider the weak formulation of equation (2.24), (2.25) or (3.25), (3.26) and to use the Lax-Migram theorem [18] instead of the Schauder's theorem in H^1 norm.

4.1 Convergence Theorem

First, we reformulate the Schauder's theorem in a way, which is convenient for our case, see §1 of Chapter 3 of [16] for this theorem.

Consider the Dirichlet boundary value problem

$$\Delta\tilde{q} + \sum_{j=1}^{3} b_j(\boldsymbol{x})\tilde{q}_{x_j} - d(\boldsymbol{x})\tilde{q} = f(x)\,, \quad x \in \Omega\,,$$

$$\tilde{q}\Big|_{\partial\Omega} = g(x) \in C^{2+\alpha}(\overline{\Omega})\,,$$

where functions

$$b_j, d, f \in C^{\alpha}(\overline{\Omega})\,, \quad d(\boldsymbol{x}) \geq 0; \quad \max\left(\|b_j\|_{C^{2+\alpha}(\overline{\Omega})}, \|d\|_{C^{2+\alpha}(\overline{\Omega})}\right) \leq M\,.$$

By the Schauder theorem there exists unique solution $\tilde{q} \in C^{2+\alpha}(\overline{\Omega})$ of this problem and with a constant $K = K(M, \Omega) > 0$ the following estimate holds

$$\|\tilde{q}\|_{C^{2+\alpha}(\overline{\Omega})} \leq K\left[\|g\|_{C^{2+\alpha}(\overline{\Omega})} + \|f\|_{C^{2+\alpha}(\overline{\Omega})}\right]\,.$$

Introduce the positive constant M^* by letting

$$B^* = 12\overline{s}^2 \cdot \max\{S^*, 1\}$$

and

$$M^* = B^* \cdot \max\left\{\max_{0\leq n\leq N}\|q_n^*\|_{C^{2+\alpha}(\overline{\Omega})}, \max_{0\leq m,n\leq N}\|q_m^*\|_{C^{2+\alpha}(\overline{\Omega})}\|q_n^*\|_{C^{2+\alpha}(\overline{\Omega})}, C^*, C_1, 2\right\}$$

where C^*, C_1 are constants and $S^* = \overline{s} - \underline{s}$.

For the tail-function, we choose a small number $\xi \in (0,1)$ and by equation (3.13) we can choose such $\overline{s}^2 = \overline{s}^2(\xi) >> 1$ such that

$$\|\bar{v}^*\|_{C^{2+\alpha}(\overline{\Omega})} \leq \xi\,.$$

Theorem 4.1

Let $\Omega \subset \mathbb{R}^2$ be a convex bounded domain with the boundary $\partial\Omega \in C^{2+\alpha}$. Suppose that an approximation v_∞ for the tail is constructed in such a way that

$$\|v_\infty\|_{C^{2+\alpha}(\overline{\Omega})} \leq \xi\,, \tag{4.1}$$

where $\xi \in (0,1)$ is a sufficient small number and that this function v_∞ is used in (2.30),(2.32), (2.33) or (3.31),(3.33), (3.34) depending on the problem. Denote $\eta = \max\{\sigma, h, \xi\}$, σ is noise level of data and h is step size, and suppose that the number $Nh = \overline{s} - \underline{s}$ is such that

$$Nh < \frac{1}{20KM^*}\,. \tag{4.2}$$

Then there exists a sufficiently small number $\eta_0 = \eta_0(K(M^*,\Omega), M^*, c, \underline{s}, \overline{s}) \in (0,1)$ such that for all $\eta \in (0,\eta_0)$ and for every integer $n \in [0, N-1]$ the following estimates hold

$$\|q_n^s - q_n^*\|_{C^{2+\alpha}(\overline{\Omega})} \leq KM^*(20\eta)\,, \tag{4.3}$$

$$\|q_n^s\|_{C^{2+\alpha}(\overline{\Omega})} \leq 2M\,. \tag{4.4}$$

4.2 Proof of Theorem

This proof basically consists of estimating the differences between our constructed functions $q_{n,k}^s$, and function q_n^*. We are doing this using the Schauder theorem. In this proof we assume that $\eta \in (0,\eta_0)$. Denote

$$\tilde{q}_{n,k}(\boldsymbol{x}) = q_{n,k}^s(\boldsymbol{x}) - q_n^*(\boldsymbol{x})\,,\ \tilde{v}_\infty(\boldsymbol{x}) = v_\infty(\boldsymbol{x}) - \bar{v}^*(\boldsymbol{x})\,,$$

$$\tilde{\psi}_n(\boldsymbol{x}) = \psi_n^s(\boldsymbol{x}) - \psi_n^*(\boldsymbol{x})\,,\ \tilde{T}_n(\boldsymbol{x}) = T_n(\boldsymbol{x}) - T_n^*(\boldsymbol{x})\,. \tag{4.5}$$

Note that, in this theorem $\|\cdot\|$ is equivalent to $\|\cdot\|_{C^{2+\alpha}(\overline{\Omega})}$. The proof basically consists of estimating these differences.

First we show the approximation of T_n, T_n^* and $\tilde{T}_n$. For $n = 1$ we have

$$\|T_1\| \leq \xi \quad , \quad \|T_1^*\| \leq \xi \quad \text{and} \quad \|\tilde{T}_1\| \leq 2\xi\,.$$

And for $n \geq 2$ we have

$$\begin{aligned} \|T_n\| &\leq h\sum_{j=0}^{n-1}\|\tilde{q}_j\| + S^* \max_{0\leq j\leq n-1}\|q_j^*\| + \xi, \\ \|T_n^*\| &\leq S^* \max_{0\leq j\leq n-1}\|q_j^*\| + \xi, \\ \|\tilde{T}_n\| &\leq h\sum_{j=0}^{n-1}\|\tilde{q}_j\| + 2\xi\,. \end{aligned}$$

Then, we estimate $\tilde{q}_0$. Subtract equation (2.41) from (2.30) or (3.42) from (3.31) depending on the problem. We obtain

$$\Delta\tilde{q}_0 + 2s_0^2\nabla\tilde{q}_0\nabla v_\infty = -2s_0^2\nabla q_0^*\nabla(v_\infty - \bar{v}^*) - 4s_0\nabla(v_\infty - \bar{v}^*)\nabla(v_\infty + \bar{v}^*) - \frac{2}{s_0}\Delta(v_\infty - \bar{v}^*)\,, \quad \text{in } \Omega \tag{4.6}$$

$$\tilde{q}_0 = \tilde{\psi}_0, \quad \text{on } \partial\Omega\,.$$

By subsection 4.1 $\|2s_0^2 v_\infty\| \leq 4\overline{s}^2\|\bar{v}^*\| \leq M^*$ and by Schauder theorem, we have

$$\|\tilde{q}_0\| \leq KM^*(5\eta)\,. \tag{4.7}$$

Hence

$$\|q_0^s\| = \|\tilde{q}_0 + q_0^*\| \leq \|\tilde{q}_0\| + \|q_0^*\| \leq KM^*(5\eta) + M^* \leq 2M^*\,. \tag{4.8}$$

Second, we estimate $\tilde{q}_{1,1}$. Set in equation (2.42) or (3.43) $n = 1$ and subtract it from (2.32) or (3.33) respectively at $n = 1, k = 1$, recalling that $q_{1,0}^s = q_0^s$. We obtain

$$\begin{aligned} &\Delta\tilde{q}_{1,1} - A_1\nabla\tilde{q}_{1,1}\nabla\tilde{q}_0 - A_1\nabla\tilde{q}_{1,1}\nabla q_0^* - B_1\nabla\tilde{q}_{1,1}\nabla\tilde{q}_0 - B_1\nabla\tilde{q}_{1,1}\nabla q_0^* - C_1\nabla\tilde{q}_{1,1}\nabla T_1 \\ &= A_1\nabla q_1^*\nabla\tilde{q}_0 + A_1\nabla q_1^*\nabla q_0^* - A_1\nabla q_1^*\nabla q_1^* + B_1\nabla q_1^*\nabla\tilde{q}_0 + C_1\nabla q_1^*\nabla\tilde{T}_1 \\ &+ D_1\Delta\tilde{q}_0 + E_1\Delta\tilde{T}_1 - F_1\nabla\tilde{q}_0\nabla\tilde{q}_0 - 2F_1\nabla\tilde{q}_0\nabla q_0^* \\ &- G_1\nabla\tilde{q}_0\nabla T_1 - G_1\nabla q_0^*\nabla\tilde{T}_1 - H_1\nabla\tilde{T}_1\nabla T_1 - H_1\nabla\tilde{T}_1\nabla T_1^* - R_1\,, \quad \text{in } \Omega \end{aligned} \tag{4.9}$$

$$q_{1,1}^s = \tilde{\psi}_1, \quad \text{on } \partial\Omega\,.$$

By subsection 4.1 $\{\|A_1\nabla\tilde{q}_0\|, \|A_1\nabla q_0^*\|, \|B_1\nabla\tilde{q}_0\|, \|B_1\nabla q_0^*\|, \|C_1\nabla T_1\|\} \leq M^*$ and by Schauder theorem, we have

$$\|\tilde{q}_{1,1}\| \leq KM^*(16\eta)\,. \tag{4.10}$$

Hence

$$\|q_{1,1}^s\| = \|\tilde{q}_{1,1} + q_1^*\| \leq \|\tilde{q}_{1,1}\| + \|q_1^*\| \leq KM^*(16\eta) + M^* \leq 2M^*\,. \tag{4.11}$$

Now we estimate $\tilde{q}_{1,k}$. Assuming that

$$\|\tilde{q}_{1,k-1}\| \leq KM^*(16\eta) \quad \text{and} \quad \|q_{1,k-1}^s\| \leq 2M^*\,. \tag{4.12}$$

Set in equation (2.42) or (3.43) $n = 1$ and subtract it from (2.32) or (3.33) respectively at $n = 1$. We obtain

$$\begin{aligned}
&\Delta\tilde{q}_{1,k} - A_1\nabla\tilde{q}_{1,k}\nabla\tilde{q}_{1,k-1} - A_1\nabla\tilde{q}_{1,k}\nabla q_0^* - B_1\nabla\tilde{q}_{1,k}\nabla\tilde{q}_0 - B_1\nabla\tilde{q}_{1,k}\nabla q_0^* - C_1\nabla\tilde{q}_{1,k}\nabla T_1 \\
&= A_1\nabla q_1^*\nabla\tilde{q}_{1,k-1} + A_1\nabla q_1^*\nabla q_0^* - A_1\nabla q_1^*\nabla q_1^* + B_1\nabla q_1^*\nabla\tilde{q}_0 + C_1\nabla q_1^*\nabla\tilde{T}_1 \\
&\quad + D_1\Delta\tilde{q}_0 + E_1\Delta\tilde{T}_1 - F_1\nabla\tilde{q}_0\nabla\tilde{q}_0 - 2F_1\nabla\tilde{q}_0\nabla q_0^* \\
&\quad - G_1\nabla\tilde{q}_0\nabla T_1 - G_1\nabla q_0^*\nabla\tilde{T}_1 - H_1\nabla\tilde{T}_1\nabla T_1 - H_1\nabla\tilde{T}_1\nabla T_1^* - R_1, \quad \text{in } \Omega, \\
&\quad q_{1,k}^s = \tilde{\psi}_1, \quad \text{on } \partial\Omega\,.
\end{aligned} \tag{4.13}$$

By subsection 4.1 $\|A_1\nabla\tilde{q}_{1,k-1}\| \leq M^*$ and by Schauder theorem, we have

$$\|\tilde{q}_{1,k}\| \leq KM^*(16\eta)\,. \tag{4.14}$$

Hence

$$|q_{1,k}^s\| = \|\tilde{q}_{1,k} + q_1^*\| \leq \|\tilde{q}_{1,k}\| + \|q_1^*\| \leq KM^*(16\eta) + M^* \leq 2M^*\,. \tag{4.15}$$

Thus we finally have

$$\|\tilde{q}_1\| \leq KM^*(16\eta) \quad \text{and} \quad \|q_1^s\| \leq 2M^*\,. \tag{4.16}$$

Now we estimate $\tilde{q}_{2,1}$. Set in equation (2.42) or (3.43) $n = 2$ and subtract it from (2.32) or (3.34) respectively at $n = 2, k = 1$, recalling that $q^s_{2,0} = q^s_1$. We obtain

$$\Delta\tilde{q}_{2,1} - A_2\nabla\tilde{q}_{2,1}\nabla\tilde{q}_1 - A_2\nabla\tilde{q}_{2,1}\nabla q^*_1 - B_2\nabla\tilde{q}_{2,1}\nabla\tilde{q}_1 - B_2\nabla\tilde{q}_{2,1}\nabla q^*_1 - C_2\nabla\tilde{q}_{2,1}\nabla T_2$$

$$= A_2\nabla q^*_2\nabla\tilde{q}_1 + A_2\nabla q^*_2\nabla q^*_1 - A_2\nabla q^*_2\nabla q^*_2 + B_2\nabla q^*_2\nabla\tilde{q}_1 + C_2\nabla q^*_2\nabla\tilde{T}_2$$

$$+D_2\Delta\tilde{q}_1 + E_2\Delta\tilde{T}_2 - F_2\nabla\tilde{q}_1\nabla\tilde{q}_1 - 2F_2\nabla\tilde{q}_1\nabla q^*_1$$

$$-G_2\nabla\tilde{q}_1\nabla T_2 - G_2\nabla q^*_1\nabla\tilde{T}_2 - H_2\nabla\tilde{T}_2\nabla T_2 - H_2\nabla\tilde{T}_2\nabla T^*_2 - R_2, \quad \text{in } \Omega, \tag{4.17}$$

$$q^s_{2,1} = \tilde{\psi}_2, \quad \text{on } \partial\Omega\,.$$

By subsection 4.1 $\{\|A_2\nabla\tilde{q}_1\|, \|A_2\nabla q^*_1\|, \|B_2\nabla\tilde{q}_1\|, \|B_2\nabla q^*_1\|, \|C_2\nabla T_2\|\} \le M^*$ and by Schauder theorem, we have

$$\|\tilde{q}_{2,1}\| \le KM^*(20\eta)\,. \tag{4.18}$$

Hence

$$\|q^s_{2,1}\| = \|\tilde{q}_{2,1} + q^*_2\| \le \|\tilde{q}_{2,1}\| + \|q^*_2\| \le KM^*(20\eta) + M^* \le 2M^*\,. \tag{4.19}$$

Now we estimate $\tilde{q}_{2,k}$. Assuming that

$$\|\tilde{q}_{2,k-1}\| \le KM^*(16\eta) \quad \text{and} \quad \|q^s_{2,k-1}\| \le 2M^*\,. \tag{4.20}$$

Set in equation (2.42) or (3.43) $n = 2$ and subtract it from (2.32) or (3.34) respectively at $n = 2$. We obtain

$$\Delta\tilde{q}_{2,k} - A_2\nabla\tilde{q}_{2,k}\nabla\tilde{q}_{2,k-1} - A_2\nabla\tilde{q}_{2,k}\nabla q^*_1 - B_2\nabla\tilde{q}_{2,k}\nabla\tilde{q}_1 - B_2\nabla\tilde{q}_{2,k}\nabla q^*_1 - C_2\nabla\tilde{q}_{2,k}\nabla T_2$$

$$= A_2\nabla q^*_2\nabla\tilde{q}_{2,k-1} + A_2\nabla q^*_2\nabla q^*_1 - A_2\nabla q^*_2\nabla q^*_2 + B_2\nabla q^*_2\nabla\tilde{q}_1 + C_2\nabla q^*_2\nabla\tilde{T}_2$$

$$+D_2\Delta\tilde{q}_1 + E_2\Delta\tilde{T}_2 - F_2\nabla\tilde{q}_1\nabla\tilde{q}_1 - 2F_2\nabla\tilde{q}_1\nabla q^*_1$$

$$-G_2\nabla\tilde{q}_1\nabla T_2 - G_2\nabla q^*_1\nabla\tilde{T}_2 - H_2\nabla\tilde{T}_2\nabla T_2 - H_2\nabla\tilde{T}_2\nabla T^*_2 - R_2, \quad \text{in } \Omega, \tag{4.21}$$

$$q^s_{2,k} = \tilde{\psi}_2, \quad \text{on } \partial\Omega\,.$$

By subsection 4.1 $\{\|A_2\nabla\tilde{q}_{2,k-1}\|\|A_2\nabla q^*_1\|, \|B_2\nabla\tilde{q}_1\|, \|B_2\nabla q^*_1\|, \|C_2\nabla T_2\|\} \le M^*$ and by Schauder theorem, we have

$$\|\tilde{q}_{2,k}\| \le KM^*(20\eta)\,. \tag{4.22}$$

Hence

$$\|q^s_{2,k}\| = \|\tilde{q}_{2,k} + q^*_2\| \le \|\tilde{q}_{2,k}\| + \|q^*_2\| \le KM^*(20\eta) + M^* \le 2M^*\,. \tag{4.23}$$

Finally we have

$$\|\tilde{q}_2\| \le KM^*(20\eta) \quad \text{and} \quad \|q^s_2\| \le 2M^*\,. \tag{4.24}$$

We now estimate the function $\tilde{q}_{n,k}$. Assume that

$$\|\tilde{q}_{n-1}\| \le KM^*(20\eta), \quad \|q^s_{n-1}\| \le 2M^* \tag{4.25}$$

and

$$\|\tilde{q}_{n,k-1}\| \le KM^*(20\eta), \quad \|q^s_{n,k-1}\| \le 2M^*\,. \tag{4.26}$$

Subtracting equation (2.42) from (2.33) or (3.43) from (3.34), we obtain

$$\begin{aligned}
&\Delta\tilde{q}_{n,k} - A_n\nabla\tilde{q}_{n,k}\nabla\tilde{q}_{n,k-1} - A_n\nabla\tilde{q}_{n,k}\nabla q^*_{n-1} - B_n\nabla\tilde{q}_{n,k}\nabla\tilde{q}_{n-1} - B_n\nabla\tilde{q}_{n,k}\nabla q^*_{n-1} - C_n\nabla\tilde{q}_{n,k}\nabla T_n \\
&= A_n\nabla q^*_n\nabla\tilde{q}_{n,k-1} + A_n\nabla q^*_n\nabla q^*_{n-1} - A_n\nabla q^*_n\nabla q^*_n + B_n\nabla q^*_n\nabla\tilde{q}_{n-1} + C_n\nabla q^*_n\nabla\tilde{T}_n \\
&\quad + D_n\Delta\tilde{q}_{n-1} + E_n\Delta\tilde{T}_n - F_n\nabla\tilde{q}_{n-1}\nabla\tilde{q}_{n-1} - 2F_n\nabla\tilde{q}_{n-1}\nabla q^*_{n-1} \\
&\quad - G_n\nabla\tilde{q}_{n-1}\nabla T_n - G_n\nabla q^*_{n-1}\nabla\tilde{T}_n - H_n\nabla\tilde{T}_n\nabla T_n - H_n\nabla\tilde{T}_n\nabla T^*_n - R_n, \quad \text{in } \Omega\,,
\end{aligned} \tag{4.27}$$

$$q^s_{n,k} = \tilde{\psi}_n, \quad \text{on } \partial\Omega\,.$$

By subsection 4.1 $\{\|A_n\nabla\tilde{q}_{n,k-1}\|, \|A_n\nabla q^*_{n-1}\|, \|B_n\nabla\tilde{q}_{n-1}\|, \|B_n\nabla q^*_{n-1}\|, \|C_n\nabla T_n\|\} \le M^*$ and by Schauder theorem, we have

$$\|\tilde{q}_{n,k}\| \le KM^*(20\eta)\,. \tag{4.28}$$

Hence

$$\|q^s_{n,k}\| = \|\tilde{q}_{n,k} + q^*_n\| \le \|\tilde{q}_{n,k}\| + \|q^*_n\| \le KM^*(20\eta) + M^* \le 2M^* \,. \tag{4.29}$$

And therefore we finally have

$$\|\tilde{q}_n\| \le KM^*(20\eta) \quad \text{and} \quad \|q^s_n\| \le 2M^* \,. \tag{4.30}$$

Estimates (4.30) complete a proof of this theorem. □

CHAPTER 5

NUMERICAL METHODS FOR THE STEADY-STATE PROBLEM

The boundary condition $w(\boldsymbol{x}, \boldsymbol{x}_0) = \varphi(\boldsymbol{x}, \boldsymbol{x}_0)$ for all $\boldsymbol{x} \in \partial\Omega$ is required to solve equation (2.1). These boundary data will be obtained from the measurement at $\partial\Omega$ by the IR Camera in actual experiments where measurement data contains a noise influence. We had presented a technique to filter these noise component by using least-square polynomial [6][7][8]. In this paper we use an alternative way of filtering noise on boundary, this idea is taken from our publication [7][9].

The simulated measurement data on the boundary of $\partial\mathcal{A}$ is generated using equation (2.1). We numerically compute the "forward problem" of equation (2.1) with condition (2.2) on Ω_0 using the finite element method (FEM) where the Dirichlet boundary condition $w_a = 36.9$ is applied on $\partial\Omega_0$. The solution of (2.1) on Ω_0 is computed with the known $a(\boldsymbol{x})$. This $a(\boldsymbol{x})$ function represents the required coefficient what is needed to perform the reconstruction stage in the inverse problem. In real experiments is obtained from the IR camera where $a(\boldsymbol{x})$ is unknown. Hence the presence of $a(\boldsymbol{x})$ in our forward problem is just for the simulation purpose. We assume that in our inverse problem, $a(\boldsymbol{x})$ is still unknown.

Once the solution $w(\boldsymbol{x}, s)$ on Ω_0 are computed, we can extract the boundary data of $\mathcal{A}$ to be our simulated measurement data for each source position s. We introduce the random noise as the random process with respect to the detector locations, this noise is added to the extracted data on $\partial\mathcal{A}$. Let $\bar{\varphi}(\boldsymbol{x}, s)$ be the extracted data on $\partial\mathcal{A}$. We compute $\widetilde{\varphi}(\boldsymbol{x}, s) = \bar{\varphi}(\boldsymbol{x}, s)[1 + \chi(\boldsymbol{x})]$ on $\partial\mathcal{A}$ where $\chi(\boldsymbol{x})$ is the random variable, which we introduce as $\chi = 0.10(w_{max} - w_{min})N$, where N is a white noise

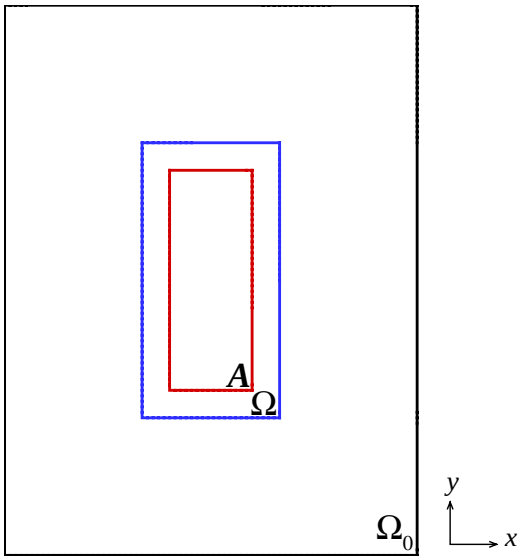

Figure 5.1. Three domains layout.

with the equal distribution at $[-1, 1]$. Hence, $\widetilde{\varphi}(\boldsymbol{x}, s)$ represents the 10% of the total difference in temperature multiplicative random noise on $\partial\mathcal{A}$. We will use this boundary data with noise as simulated data in our inverse problem. Figure 5.1 illustrates computation domains Ω_0 and $\mathcal{A}$.

After the forward problem of equation (2.1) in Ω_0 is solved, we assign the measurement data plus noise on $\partial\mathcal{A}$ as the Dirichlet condition. Then we solve the exterior forward problem in $\Omega_0 \backslash \mathcal{A}$ with the Robin boundary condition on $\partial\Omega_0$. Function $a(\boldsymbol{x})$ in $\Omega_0 \backslash \mathcal{A}$ is set to the background value k^2. The boundary data for inverse problem is extracted along the $\partial\Omega$, see figure 5.1.

The numerical computation for inverse problem in Ω domain begins with the computation of tail function, detail of derivation and computation can be founded on subsection 7.2 "An enhanced tail function" on [9]. Once we have the tail function, we

compute the numerical layer stripping in Section 2.2. Since the convergence of this technique has been proved for $q_n^s(\boldsymbol{x})$ for all $s \in [s_n, s_{n-1})$. In this computation, we set $s = s_n$, this makes $q_n^s(\boldsymbol{x}) = q_n(\boldsymbol{x})$. Then the backward substitution is performed to obtain the target coefficient $a(\boldsymbol{x})$.

5.1 A Mathematical Model of the Tail for the Steady-State Problem

First, we consider the fundamental solution of the 2D diffusion equation for the case $a(\boldsymbol{x}) \equiv k^2$ where k^2 is background value of our domain, or we simply say the case with no inclusions in domain Ω. This solution is

$$\widetilde{w}_0(\boldsymbol{x}, s) = \frac{1}{2\pi} K_0(ks') \tag{5.1}$$

where K_0 is a modified Bessel function and $s' = |(x - B, y - s)|$, see figure 5.2. Its asymptotic behaviors is

$$K_0(ks') = \sqrt{\frac{\pi}{2s'}} e^{-ks'} \Big[1 + O(\frac{1}{s'})\Big] \quad , \ s' \to \infty \,. \tag{5.2}$$

Represent solution of equation (2.4) with

$$w(\boldsymbol{x}, s) = \widetilde{w}_0(\boldsymbol{x}, s) + W(\boldsymbol{x}, s) \,. \tag{5.3}$$

Since $\widetilde{w}_0$ satisfies $\Delta\widetilde{w}_0 - k^2\widetilde{w}_0 = 0$ in Ω, then equation (2.4) becomes

$$\Delta W - [a(\boldsymbol{x}) - k^2]\widetilde{w}_0 - [a(\boldsymbol{x}) - k^2]W - k^2 W = 0 \,. \tag{5.4}$$

Therefore we have

$$\Delta W - k^2 W = [a(\boldsymbol{x}) - k^2]w \,. \tag{5.5}$$

This is the *Inhomogeneous Helmholtz* equation where the solution can be written as follows

$$W(\boldsymbol{x}, s) = -\frac{1}{2\pi} \int_\Omega K_0 \left(k|\boldsymbol{x} - \xi|\right) [a(\xi) - k^2] w(\xi, s) \, d\xi \,. \tag{5.6}$$

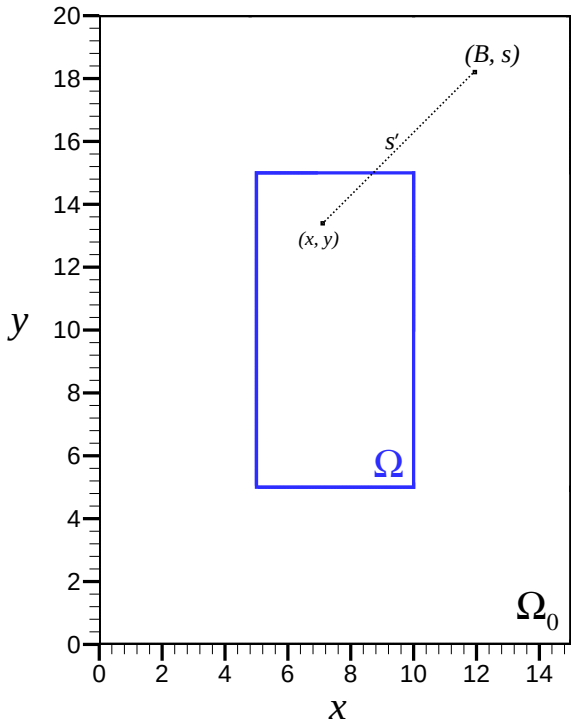

Figure 5.2. Distance of light source $s' = |(x - B, y - s)|$.

Substituting equation (5.6) into equation (5.3), the solution of equation (2.4) becomes the following integral equation

$$w(\boldsymbol{x}, s) = \widetilde{w}_0(\boldsymbol{x}, s) - \frac{1}{2\pi} \int_\Omega K_0 \left(k|\boldsymbol{x} - \xi|\right) [a(\xi) - k^2] w(\xi, s)\, d\xi \,. \tag{5.7}$$

We introduce the function

$$\overline{W}(\boldsymbol{x}, s) = 2\sqrt{2\pi s'} e^{ks'} w(\boldsymbol{x}, s) \,. \tag{5.8}$$

Hence, multiplication of $\sqrt{s'} e^{ks'}$ to equation (5.7) gives

$$\overline{W}(\boldsymbol{x}, s) = \left[1 + O(\frac{1}{s'})\right] - \frac{1}{2\pi} \int_\Omega K_0 \left(c|\boldsymbol{x} - \xi|\right) [a(\xi) - k^2] \frac{2\sqrt{2\pi s'} e^{ks'}}{2\sqrt{2\pi \tilde{s}} e^{k\tilde{s}}} \overline{W}(\xi, s)\, d\xi \,, \tag{5.9}$$

where $\tilde{s} = |\xi - s|$, $s = (B, s)$. From equation (5.9), we have the asymptotic term

$$\frac{\sqrt{s'} e^{ks'}}{\sqrt{\tilde{s}} e^{k\tilde{s}}} \to 1 \quad \text{as} \quad s \to \infty \,.$$

Therefore $\overline{W}$ has a unique solution decaying at infinity, and equation (5.9) becomes

$$\overline{W}(\boldsymbol{x}, s) = 1 + \tilde{g}(\boldsymbol{x}) + O(\frac{1}{s'}) \quad , \text{ as } s' \to \infty \,. \tag{5.10}$$

Another form of equation (5.10) based on equation (5.8) is the asymptotic behavior of w as $s' \to \infty$

$$w(\boldsymbol{x}, s) = \frac{e^{-ks'}}{2\sqrt{2\pi s'}}(1 + \tilde{g}(\boldsymbol{x}) + O(\frac{1}{s'})) \quad , \text{ as } s' \to \infty \,. \tag{5.11}$$

The function $\tilde{g}(\boldsymbol{x})$ is unknown and is independent of s'. Since we are interested in the function $u = \ln w$, we have

$$u(\boldsymbol{x}, s) = -ks' - \ln 2\sqrt{2\pi} - \frac{1}{2}\ln s' + g(\boldsymbol{x}) + O(\frac{1}{s'}) \quad , \text{ as } s' \to \infty \,, \tag{5.12}$$

where $g(\boldsymbol{x})$ is also independent of s'. If we can approximate $g(\boldsymbol{x})$ we can also approximate $u(\boldsymbol{x}, s)$ and hence $v(\boldsymbol{x}, s)$. Since function $u(\boldsymbol{x}, s)$ can be obtained only at the boundary, no information of $u(\boldsymbol{x}, s)$ within the interior of Ω, we will explain the heuristic approach of approximating $g(\boldsymbol{x})$ with the incomplete $u(\boldsymbol{x}, s)$ in the next section.

5.2 The First Guess of the Tail for the Steady-State Problem

In the steady-state problem we approximate the tail function using four different angles, see figure 8.1 for the locations of the heat sources. Angle #1 is used for the computation of the inverse problem while all four angles are used for the computation of the tail function. Let $w_0(\boldsymbol{x}, s)$ be the solution of

$$\Delta \widetilde{w}_0 - k^2 \widetilde{w}_0 = 0 \tag{5.13}$$

where k^2 is the background value of $a(\boldsymbol{x})$. From equation (5.12), we have

$$\ln(w(\boldsymbol{x}, s)) = \ln(\widetilde{w}_0(\boldsymbol{x}, s)) + g(\boldsymbol{x}) \tag{5.14}$$

Now we need to compute $g^{(n)}(\boldsymbol{x})$, n=1,2,3,4, in Ω which represent four different functions each derived from a different angle.

1) To compute $g^{(1)}(\boldsymbol{x})$ based upon angle #1 we need to compute $g_i^{(1)}(\boldsymbol{x})$ for each s_i $i = 0, ..., 4$. For the left boundary we fix x_1 on the left boundary of Ω

$$g_i^{(1)}(x_1, y) = \ln(w(x_1, y, s_i)) - \ln(\widetilde{w}_0(x_1, y, s_i)) \tag{5.15}$$

and for the bottom boundary we fix y_1 on the bottom boundary to get

$$g_i^{(1)}(x, y_1) = \ln(w(x, y_1, s_i)) - \ln(\widetilde{w}_0(x, y_1, s_i)) \tag{5.16}$$

Now

$$g^{(1)}(x_1, y) = \frac{1}{5}\sum_{i=0}^{4} g_i^{(1)}(x_1, y) \tag{5.17}$$

$$g^{(1)}(x, y_1) = \frac{1}{5}\sum_{i=0}^{4} g_i^{(1)}(x, y_1) \tag{5.18}$$

Finally we have that

$$g^{(1)}(x, y) = \frac{1}{2}(g^{(1)}(x_1, y) + g^{(1)}(y_1, x)) \tag{5.19}$$

2) To compute $g^{(2)}(\boldsymbol{x})$ based upon angle #2 we need to compute $g_2^{(1)}(\boldsymbol{x})$ for each s_i $i = 5, ..., 7$. For the left boundary we fix x_1 on the left boundary of Ω

$$g_i^{(2)}(x_1, y) = \ln(w(x_1, y, s_i)) - \ln(\widetilde{w}_0(x_1, y, s_i)) \tag{5.20}$$

and for the top boundary we fix y_2 on the top boundary to get

$$g_i^{(2)}(x, y_2) = \ln(w(x, y_2, s_i)) - \ln(\widetilde{w}_0(x, y_2, s_i)) \tag{5.21}$$

Now

$$g^{(2)}(x_1, y) = \frac{1}{3}\sum_{i=5}^{7} g_i^{(2)}(x_1, y) \tag{5.22}$$

$$g^{(2)}(x, y_2) = \frac{1}{3}\sum_{i=5}^{7} g_i^{(2)}(x, y_2) \tag{5.23}$$

Finally we have that

$$g^{(2)}(x, y) = \frac{1}{2}(g^{(1)}(x_1, y) + g^{(1)}(x, y_2)) \tag{5.24}$$

3) To compute $g^{(3)}(\boldsymbol{x})$ based upon angle #3 we need to compute $g_i^{(3)}(\boldsymbol{x})$ for each s_i $i = 8, ..., 10$. For the right boundary we fix x_2 on the right boundary of Ω

$$g_i^{(3)}(x_2, y) = \ln(w(x_2, y, s_i)) - \ln(\widetilde{w}_0(x_2, y, s_i)) \tag{5.25}$$

and for the bottom boundary we fix y_1 on the bottom boundary to get

$$g_i^{(3)}(x, y_1) = \ln(w(x, y_1, s_i)) - \ln(\widetilde{w}_0(x, y_1, s_i)) \tag{5.26}$$

Now

$$g^{(3)}(x_2, y) = \frac{1}{3}\sum_{i=8}^{10} g_i^{(3)}(x_2, y) \tag{5.27}$$

$$g^{(3)}(x, y_1) = \frac{1}{3}\sum_{i=8}^{10} g_i^{(3)}(x, y_1) \tag{5.28}$$

Finally we have that

$$g^{(3)}(x, y) = \frac{1}{2}(g^{(3)}(x_2, y) + g^{(3)}(x, y_1)) \tag{5.29}$$

4) To compute $g^{(4)}(\boldsymbol{x})$ based upon angle #4 we need to compute $g_i^{(4)}(\boldsymbol{x})$ for each s_i $i = 11, ..., 13$. For the right boundary we fix x_2 on the right boundary of Ω

$$g_i^{(4)}(x_2, y) = \ln(w(x_2, y, s_i)) - \ln(\widetilde{w}_0(x_2, y, s_i)) \tag{5.30}$$

and for the top boundary we fix y_2 on the top boundary to get

$$g_i^{(4)}(x, y_2) = \ln(w(x, y_2, s_i)) - \ln(\widetilde{w}_0(x, y_2, s_i)) \tag{5.31}$$

. Now

$$g^{(4)}(x_2, y) = \frac{1}{3}\sum_{i=11}^{13} g_i^{(4)}(x_2, y) \tag{5.32}$$

$$g^{(4)}(x, y_2) = \frac{1}{3}\sum_{i=11}^{13} g_i^{(4)}(x, y_2) \tag{5.33}$$

Finally we have that

$$g^{(4)}(x, y) = \frac{1}{2}(g^{(4)}(x_2, y) + g^{(4)}(x, y_2)) \tag{5.34}$$

Once we know $g^{(n)}$, $n = 1, 2, 3, 4$, we compute $u^{(n)}$, $n = 1, 2, 3, 4$, which represent the first guess of tail from each angle. We compute them by

$$\begin{aligned}
u^{(1)}(\boldsymbol{x}) &= \ln \widetilde{w}_0(\boldsymbol{x}, s_0) + g^{(1)}(\boldsymbol{x}),\\
u^{(2)}(\boldsymbol{x}) &= \ln \widetilde{w}_0(\boldsymbol{x}, s_5) + g^{(2)}(\boldsymbol{x}),\\
u^{(3)}(\boldsymbol{x}) &= \ln \widetilde{w}_0(\boldsymbol{x}, s_8) + g^{(3)}(\boldsymbol{x}),\\
u^{(4)}(\boldsymbol{x}) &= \ln \widetilde{w}_0(\boldsymbol{x}, s_{11}) + g^{(4)}(\boldsymbol{x}),
\end{aligned}$$

on Ω where s_0, s_5, s_8 and s_{11} are the farthest heat source locations of each angle. Then we compute function $w^{(i)}(\boldsymbol{x}) = \exp\left(u^{(i)}(\boldsymbol{x})\right)$, $i = 1, 2, 3, 4$ and solve for $a^{(i)}$ from the equation

$$\Delta w^{(i)}(\boldsymbol{x}) - a^{(i)}(\boldsymbol{x}) w^{(i)}(\boldsymbol{x}) = 0$$

by the weak form of FEM. Let η be the test function. Multiplying both side of above equation by η and integrating over Ω. We obtain

$$\int_\Omega \eta \Delta w^{(i)}\, d\boldsymbol{x} - \int_\Omega \eta a^{(i)} w^{(i)}\, d\boldsymbol{x} = 0$$

or equivalently

$$\int_{\partial\Omega} \eta(\vec{n}\cdot\nabla w^{(i)})\, d\boldsymbol{x} - \int_\Omega \nabla\eta\cdot\nabla w^{(i)}\, d\boldsymbol{x} - \int_\Omega \eta a^{(i)} w^{(i)}\, d\boldsymbol{x} = 0\,.$$

Since the Robin condition is zero on domain Ω, the first terms is dropped. We then numerically solve the weak form of the following equation

$$\int_\Omega \nabla\eta \cdot \nabla w^{(i)}\, d\boldsymbol{x} + \int_\Omega \eta a^{(i)} w^{(i)}\, d\boldsymbol{x} = 0, \quad , \quad a^{(i)} = k^2 \text{ on } \partial\Omega\,.$$

After $a^{(i)}$, $i = 1, 2, 3, 4$ are computed, we average them to get a_{tail} by

$$a_{\text{tail}}(\boldsymbol{x}) = \frac{1}{4}[a^{(1)}(\boldsymbol{x}) + a^{(2)}(\boldsymbol{x}) + a^{(3)}(\boldsymbol{x}) + a^{(4)}(\boldsymbol{x})], \quad \text{where } \boldsymbol{x} \in \Omega\,. \tag{5.35}$$

We solve using the FEM equation to obtain a smooth tail function w_{tail} on Ω by

$$\int_\Omega \nabla\eta \cdot \nabla w_{\text{tail}}\, d\boldsymbol{x} + \int_\Omega \eta a_{\text{tail}} w_{\text{tail}}\, d\boldsymbol{x} = 0, \quad , \quad w_{\text{tail}} = \varphi(\boldsymbol{x}, s_0) \text{ on } \partial\Omega\,.$$

Note that, $s_0 = \overline{s}$ which is the farthest light source in our layer stripping, see Section 2.2.

We compute the first guess for tails

$$\bar{v}_0(\boldsymbol{x}) = \frac{\bar{u}_0(\boldsymbol{x})}{\overline{s}^2} = \frac{\ln w_{\text{tail}}}{\overline{s}^2}, \quad \boldsymbol{x} \in \Omega\,. \tag{5.36}$$

This tail $\bar{v}_0(\boldsymbol{x})$ is known as the first guess. By using $\bar{v}_0(\boldsymbol{x})$ as a tail function for the inverse problem, it has provided most of the information about locations of the inclusions. These locations were reconstructed precisely. However the peak value of the reconstructed coefficient within inclusions was too low compared to the peak of original inclusions. Hence an iteration procedure for improving the quality of $\bar{v}_0(\boldsymbol{x})$ is required and is explained in the following section.

An improving procedure in this section is introduced to calibrate the tail function, so that its limiting solution (when it exists) will satisfy the original diffusion model. This involves an iterative process that enhances the reconstructed inclusion. This idea is motivated by letting the following two diffusion equation be evaluated at light source $\boldsymbol{x}_0 = (B, \overline{s})$

$$\Delta\bar{w}_{i-1} - a_{i-1}\bar{w}_{i-1} = -\delta(\boldsymbol{x} - \boldsymbol{x}_0)\,, \tag{5.37}$$

$$\Delta \bar{w}_i - a_i \bar{w}_i = -\delta(\boldsymbol{x} - \boldsymbol{x}_0)\,. \tag{5.38}$$

The difference of the above two equations can be written as follows

$$\Delta p_i - a_i p_i = (a_i - a_{i-1})\bar{w}_{i-1}\,. \tag{5.39}$$

where $p_i = \bar{w}_i - \bar{w}_{i-1}$. The purpose of this iteration scheme is to improve the quality of $w(\boldsymbol{x}, \overline{s})$. We expect that $\bar{w}_i(\boldsymbol{x}, \overline{s})$ will converge to a value close to the exact value $w^*(\boldsymbol{x}, \overline{s})$ discussed in subsection 2.3 resulting in the tail function $v_\infty(\boldsymbol{x})$ which is close to $v^*(\boldsymbol{x}, \overline{s})$.

CHAPTER 6

NUMERICAL METHODS FOR THE TIME DEPENDENT PROBLEM

The boundary condition $w(\boldsymbol{x}, \boldsymbol{x}_0) = \varphi(\boldsymbol{x}, \boldsymbol{x}_0)$ for all $\boldsymbol{x} \in \partial\Omega$ is required to solve equation (1.1). These boundary data will be obtained from the measurement at $\partial\Omega$ by the ICCD Camera in actual experiments where measurement data contains a noise influence.

The simulated measurement data on $\partial\mathcal{A}$ is generated using equation (3.5). We numerically compute the "forward problem" of equation (3.5) using the finite element method (FEM) where the Robin boundary condition $\vec{n} \cdot \nabla w(\boldsymbol{x}, s) + w(\boldsymbol{x}, s) = 0$ is applied on $\partial\Omega_0$. The solution of (3.5) on Ω_0 is computed with the known $a(\boldsymbol{x})$. This $a(\boldsymbol{x})$ function represents the required coefficient what is needed to perform the reconstruction stage in the inverse problem. In real experiments is obtained from the ICCD camera where $a(\boldsymbol{x})$ is unknown.

Once the solution $\tilde{u}(\boldsymbol{x}, s)$ on Ω_0 are computed, we can extract the boundary data of $\mathcal{A}$ to be our simulated measurement data for each frequency s. We introduce the random noise as the random process with respect to the detector locations, this noise is added to the extracted data on $\partial\mathcal{A}$. Let $\bar{\varphi}(\boldsymbol{x}, s)$ be the extracted data on $\partial\mathcal{A}$. We compute $\widetilde{\varphi}(\boldsymbol{x}, s) = \bar{\varphi}(\boldsymbol{x}, s)[1 + \chi(\boldsymbol{x})]$ on $\partial\mathcal{A}$ where $\chi(\boldsymbol{x})$ is the random variable, which we introduce as $\chi = 0.05N$, where N is a white noise with the equal distribution at $[-1, 1]$. Hence, $\widetilde{\varphi}(\boldsymbol{x}, s)$ represents the multiplicative random noise on $\partial\mathcal{A}$. We will use this boundary data with noise as simulated data in our inverse problem. Figure 5.1 illustrates computation domains Ω_0 and $\mathcal{A}$.

6.1 A Mathematical Model of the Tail for the Time-Dependent Problem

In our globally convergent method the first step is to get an approximation of our tail function, $v(\boldsymbol{x}, \overline{s})$. This method for computing the tail is similar to the construction of the tail function in the steady state problem in the sense that we investigate the fundamental solution of the problem with the background value of $a(\boldsymbol{x})$ and consider the source position to be far enough away to give the desired asymptotic behavior. We consider the fundamental solution of the 2D diffusion equation for the case $a(\boldsymbol{x}) + s^2 \equiv \widetilde{k}^2 + s^2 = k^2$ where $\widetilde{k}^2$ is background value of our domain, or we simply say the case with no inclusions in domain Ω. This solution is

$$\widetilde{u}_0(\boldsymbol{x}, s) = \frac{1}{2\pi} K_0(kd') \tag{6.1}$$

where K_0 is a modified Bessel function and $d' = |x - x_0|$. Its asymptotic behaviors is

$$K_0(kd') = \sqrt{\frac{\pi}{2d'}} e^{-kd'} \Big[1 + O(\frac{1}{d'})\Big],\ d' \to \infty\,. \tag{6.2}$$

Represent solution of equation (3.5) with

$$\tilde{u}(\boldsymbol{x}, s) = \widetilde{u}_0(\boldsymbol{x}, s) + U(\boldsymbol{x}, s), \tag{6.3}$$

where $\widetilde{u}_0$ satisfies $\Delta\widetilde{u}_0 - (s^2 + \widetilde{k}^2)\widetilde{u}_0 = 0$ in Ω, then equation (3.5) becomes

$$\Delta U - [a(\boldsymbol{x}) - \widetilde{k}^2]\widetilde{u}_0 - [a(\boldsymbol{x}) - \widetilde{k}^2]U - k^2 U = 0\,. \tag{6.4}$$

Therefore we have

$$\Delta U - k^2 U = [a(\boldsymbol{x}) - \widetilde{k}^2]\tilde{u}\,. \tag{6.5}$$

This is the *Inhomogeneous Helmholtz* equation where the solution can be written as follows

$$U(\boldsymbol{x}, s) = -\frac{1}{2\pi} \int_\Omega K_0\left(k|\boldsymbol{x} - \xi|\right) [a(\xi) - \widetilde{k}^2]\tilde{u}(\xi, s)\, d\xi\,. \tag{6.6}$$

Substituting equation (6.6) into equation (6.3), the solution of equation (3.5) becomes the following integral equation

$$\tilde{u}(\boldsymbol{x},s) = \widetilde{u}_0(\boldsymbol{x},s) - \frac{1}{2\pi}\int_\Omega K_0\left(k|\boldsymbol{x}-\xi|\right)[a(\xi)-\widetilde{k}^2]\tilde{u}(\xi,s)\,d\xi\,. \tag{6.7}$$

We introduce the function

$$\overline{U}(\boldsymbol{x},s) = 2\sqrt{2\pi d'}e^{kd'}\tilde{u}(\boldsymbol{x},s)\,. \tag{6.8}$$

Hence, multiplication of $\sqrt{d'}e^{kd'}$ to equation (6.7) gives

$$\overline{U}(\boldsymbol{x},s) = \Big[1+O(\frac{1}{d'})\Big] - \frac{1}{2\pi}\int_\Omega K_0\left(k|\boldsymbol{x}-\xi|\right)[a(\xi)-\widetilde{k}^2]\frac{2\sqrt{2\pi d'}e^{kd'}}{2\sqrt{2\pi\tilde{d}}e^{k\tilde{d}}}\overline{U}(\xi,s)\,d\xi\,, \tag{6.9}$$

where $\tilde{d} = |\xi - x_0|$. From equation (6.9), we have the asymptotic term

$$\frac{\sqrt{d'}e^{kd'}}{\sqrt{\tilde{d}}e^{k\tilde{d}}} \to 1 \quad \text{as} \quad \boldsymbol{x}_0 \to \infty\,.$$

Therefore $\overline{U}$ has a unique solution decaying at infinity, and equation (6.9) becomes

$$\overline{U}(\boldsymbol{x},s) = 1 + \tilde{g}(\boldsymbol{x}) + O(\frac{1}{d'}) \quad , \text{ as } \boldsymbol{x}_0 \to \infty\,. \tag{6.10}$$

Another form of equation (6.10) based on equation (6.8) is the asymptotic behavior of $\tilde{u}$ as $\boldsymbol{x}_0 \to \infty$

$$\tilde{u}(\boldsymbol{x},s) = \frac{e^{-kd'}}{2\sqrt{2\pi d'}}(1+\tilde{g}(\boldsymbol{x})+O(\frac{1}{d'})) \quad , \text{ as } \boldsymbol{x}_0 \to \infty\,. \tag{6.11}$$

The function $\tilde{g}(\boldsymbol{x})$ is unknown and is independent of d'. Since we are interested in the function $u = \ln\tilde{u}$, we have

$$u(\boldsymbol{x},s) = -kd' - \ln 2\sqrt{2\pi} - \frac{1}{2}\ln d' + g(\boldsymbol{x}) + O(\frac{1}{d'}),\ \text{as } \boldsymbol{x}_0 \to \infty\,, \tag{6.12}$$

where $g(\boldsymbol{x})$ is also independent of d'. If we can approximate $g(\boldsymbol{x})$ we can also approximate $u(\boldsymbol{x},s)$ and hence $v(\boldsymbol{x},s)$. Since function $g(\boldsymbol{x})$ can be obtained only at the boundary the interior of Ω needs to be approximated by extrapolation of $g(\boldsymbol{x})$, $\boldsymbol{x} \in \partial\Omega$.

6.2 A Mathematical Model of the Tail for the Time-Dependent Problem after Rescaling

In many applications such as optical tomography the assumption that the source position is far away from the domain of reconstruction does not match the physical reality of the problem. To compensate for this problem we can alter the scale of the domain using the frequency and allow the magnitude of the frequency to get the desired asymptotic behavior. After the Laplace-like Transform we have

$$\Delta_x \tilde{u} - (s^2 + a(x))\tilde{u} = -\delta(x - x_0). \tag{6.13}$$

Let $x = \frac{x'}{s}$. Thus

$$s^2 \Delta_{x'} \tilde{u} - (s^2 + a(x))\tilde{u} = -\delta(\frac{x' - x_0 s}{s}). \tag{6.14}$$

After re-scaling the delta function we have

$$s^2 \Delta_{x'} \tilde{u} - (s^2 + a(x))\tilde{u} = -s\delta(x' - x_0 s). \tag{6.15}$$

Divide by s^2 to get

$$\Delta_{x'} \tilde{u} - (1 + \frac{a(x)}{s^2})\tilde{u} = -\frac{\delta(x' - x_0 s)}{s}. \tag{6.16}$$

Let $\tilde{u} = \frac{f}{s}$ and we have

$$\Delta_{x'} f - (1 + \frac{a(x)}{s^2}) f = -\delta(x' - x_0 s). \tag{6.17}$$

We consider the fundamental solution as $s \to \infty$ to remove the influence of the target coefficient and consider the following equation.

$$\Delta f_0 - f_0 = -\delta(x' - s x_0). \tag{6.18}$$

For homogeneous media, the fundamental solution is

$$f_0 = \frac{1}{2\pi} K_0(c') \tag{6.19}$$

in R^2 where K_0 is a modified Bessel function and $c' = |x' - sx_0|$. It's asymptotic behavior is

$$K_0(c') = \sqrt{\frac{\pi}{2c'}} e^{-c'}(1 + O(\frac{1}{c'})), c' \to \infty. \tag{6.20}$$

Let $f = f_0 + F$ since f_0 satisfies $\Delta f_0 - f_0 = 0$ in Ω. Then equation (6.17) becomes

$$\Delta F - F = \frac{a(x)}{s^2} f \text{ in } \Omega. \tag{6.21}$$

This is the *Inhomogeneous Helmholtz* equation where the solution can be written as

$$F(x,s) = -\frac{1}{2\pi} \int_\Omega K_0(|x-\xi|)\,[\frac{a(\xi)}{s^2}] f(\xi,s)\,d\xi\,. \tag{6.22}$$

Thus

$$f(x,s) = f_0(x,s) - \frac{1}{2\pi} \int_\Omega K_0(|x-\xi|)\,[\frac{a(\xi)}{s^2}] f(\xi,s)\,d\xi\,. \tag{6.23}$$

We now introduce the function

$$\overline{F}(x,s) = 2\sqrt{2\pi c'} e^{c'} f(x,s) \tag{6.24}$$

Hence, multiplication of $2\sqrt{2\pi c'}e^{c'}$ to equation (6.23) gives

$$\overline{F}(x,s) = 1 + O(\frac{1}{c'}) - \frac{1}{2\pi} \int_\Omega K_0(c|x-\xi|)\,[\frac{a(\xi)}{s^2}] \frac{2\sqrt{2\pi c'}e^{c'}}{2\sqrt{2\pi\tilde{c}}e^{\tilde{c}}} \overline{F}(\xi,s)\,d\xi\,. \tag{6.25}$$

where $\tilde{c} = |\xi - x_0 s|$. Considering

$$\frac{2\sqrt{2\pi c'}e^{c'}}{2\sqrt{2\pi\tilde{c}}e^{\tilde{c}}} \to 1 \quad \text{as} \quad s \to \infty \tag{6.26}$$

We obtain that $\overline{F}$ has a unique solution decaying at infinity, and equation (6.25) becomes

$$\overline{F}(x,s) = 1 + \hat{g}(x) + O(\frac{1}{c'}). \tag{6.27}$$

The asymptotic behavior of f as $sx_0 \to \infty$ is

$$f(\boldsymbol{x},s) = \frac{e^{-c'}}{2\sqrt{2\pi c'}}(1 + \hat{g}(\boldsymbol{x}) + O(\frac{1}{c'})), \text{ as } sx_0 \to \infty\,. \tag{6.28}$$

Then

$$\tilde{u}(\boldsymbol{x}, s) = \frac{e^{-c'}}{2\sqrt{2\pi c'}s}(1 + \hat{g}(\boldsymbol{x}) + O(\frac{1}{c'})), \text{ as } sx_0 \to \infty\,. \tag{6.29}$$

The function $\hat{g}(\boldsymbol{x})$ is unknown and is independent of c' as $c' \to \infty$. Since we are interested in the function $u = \ln \tilde{u}$, we have

$$u(\boldsymbol{x}, s) = -c' - \ln 2\sqrt{2\pi} - \frac{1}{2}\ln c' - \ln(s) + g(\boldsymbol{x}) + O(\frac{1}{c'}), \text{ as } sx_0 \to \infty\,. \tag{6.30}$$

If we can approximate $g(\boldsymbol{x})$ we can also approximate $u(\boldsymbol{x}, s)$ and hence $v(\boldsymbol{x}, s)$. Since function $g(x)$ can be obtained only at the boundary the interior of Ω needs to be approximated by extrapolation of $g(x)$, $x \in \Omega$. In this current model both tail functions yielded the similar results however in other applications of this GCM that may not be the case.

6.3 The First Guess of the Tail for the Time-Dependent Problem

In the time-dependent problem we approximate the tail function using only two angles, see figure 9.1 for the locations of the light sources. Angle #1 is used for the computation of the inverse problem while both angles are used for the computation of the tail function.

$$\ln(\tilde{u}(\boldsymbol{x}, s)) = \ln(\tilde{u}_0(\boldsymbol{x}, s)) + g(\boldsymbol{x}) \tag{6.31}$$

or

$$\ln(\tilde{u}(\boldsymbol{x}, s)) = \ln(f_0(\boldsymbol{x}, s)/s) + g(\boldsymbol{x}) \tag{6.32}$$

for the rescaled time-dependent problem. In either case $g(\boldsymbol{x})$ is constructed in the same manner so in this section we will focus just on the problem that was not rescaled. Now we need to compute $g^{(n)}(\boldsymbol{x})$, n=1,2, in Ω which represent two different functions each derived from a different angle where x_1', x_2' will represent the two source positions.

1) To compute $g^{(1)}(\boldsymbol{x})$ based upon angle #1 we need to compute $g_i^{(1)}(\boldsymbol{x})$ for each s_i $i = 0, ..., N-1$. For the left boundary we fix x_1 on the left boundary of Ω

$$g_i^{(1)}(x_1, y) = \ln(\tilde{u}(x_1, y, s_i, x_1')) - \ln(\tilde{u}_0(x_1, y, s_i, x_1')) \tag{6.33}$$

and for the bottom boundary we fix y_1 on the bottom boundary to get

$$g_i^{(1)}(x, y_1) = \ln(\tilde{u}(x, y_1, s_i, x_1')) - \ln(\tilde{u}_0(x, y_1, s_i, x_1')). \tag{6.34}$$

Now

$$g^{(1)}(x_1, y) = \frac{1}{N} \sum_{i=0}^{N-1} g_i^{(1)}(x_1, y), \tag{6.35}$$

$$g^{(1)}(x, y_1) = \frac{1}{N} \sum_{i=0}^{N-1} g_i^{(1)}(x, y_1). \tag{6.36}$$

Finally we have that

$$g^{(1)}(x, y) = \frac{1}{3}(2g^{(1)}(x_1, y) + g^{(1)}(y_1, x)). \tag{6.37}$$

2) To compute $g^{(2)}(\boldsymbol{x})$ based upon angle #2 we need to compute $g_2^{(1)}(\boldsymbol{x})$ for each s_i $i = 0, ..., N-1$. For the right boundary we fix x_2 on the right boundary of Ω

$$g_i^{(2)}(x_2, y) = \ln(\tilde{u}(x_2, y, s_i, x_2')) - \ln(\tilde{u}_0(x_2, y, s_i, x_2')) \tag{6.38}$$

and for the top boundary we fix y_2 on the top boundary to get

$$g_i^{(2)}(x, y_2) = \ln(\tilde{u}(x, y_2, s_i x_2')) - \ln(\tilde{u}_0(x, y_2, s_i, x_2')). \tag{6.39}$$

Now

$$g^{(2)}(x_2, y) = \frac{1}{N} \sum_{i=0}^{N-1} g_i^{(2)}(x_2, y), \tag{6.40}$$

$$g^{(2)}(x, y_2) = \frac{1}{N} \sum_{i=0}^{N-1} g_i^{(2)}(x, y_2). \tag{6.41}$$

Finally we have that

$$g^{(2)}(x,y) = \frac{1}{3}(2g^{(2)}(x_2,y) + g^{(2)}(y_2,x)). \tag{6.42}$$

Once we know $g^{(n)}$, $n = 1, 2$, we compute $u^{(n)}$, $n = 1, 2, 3, 4$, which represent the first guess of tail from each angle. We compute them by

$$\begin{aligned} u^{(1)}(\boldsymbol{x}) &= \ln \tilde{u}_0(\boldsymbol{x}, s_0, x_1') + g^{(1)}(\boldsymbol{x}), \\ u^{(2)}(\boldsymbol{x}) &= \ln \tilde{u}_0(\boldsymbol{x}, s_0, x_2') + g^{(2)}(\boldsymbol{x}). \end{aligned}$$

Then we compute function $\tilde{u}^{(i)}(\boldsymbol{x}) = \exp\left(u^{(i)}(\boldsymbol{x})\right)$, $i = 1, 2$ and solve for $a^{(i)} + s_0^2$ from the equation

$$\Delta\tilde{u}^{(i)}(\boldsymbol{x}) - (a^{(i)}(\boldsymbol{x}) + s_0^2)\tilde{u}^{(i)}(\boldsymbol{x}) = 0$$

by the weak form of FEM. Let η be the test function. Multiplying both side of above equation by η and integrating over Ω. We obtain

$$\int_\Omega \eta\Delta\tilde{u}^{(i)}\, d\boldsymbol{x} - \int_\Omega \eta(a^{(i)} + s_0^2)\tilde{u}^{(i)}\, d\boldsymbol{x} = 0$$

or

$$\int_{\partial\Omega} \eta(\vec{n}\cdot\nabla\tilde{u}^{(i)})\, d\boldsymbol{x} - \int_\Omega \nabla\eta\cdot\nabla\tilde{u}^{(i)}\, d\boldsymbol{x} - \int_\Omega \eta(a^{(i)} + s_0^2)\tilde{u}^{(i)}\, d\boldsymbol{x} = 0\,.$$

Since the Robin condition is zero on domain Ω, the first terms is dropped. We then numerically solve the weak form of the following equation

$$\int_\Omega \nabla\eta\cdot\nabla\tilde{u}^{(i)}\, d\boldsymbol{x} + \int_\Omega \eta(a^{(i)} + s_0^2)\tilde{u}^{(i)}\, d\boldsymbol{x} = 0, \quad a^{(i)} = \tilde{k}^2 \text{ on } \partial\Omega\,.$$

After $a^{(i)}$, $i = 1, 2$ are computed, we average them to get a_{tail} by

$$a_{\text{tail}}(\boldsymbol{x}) = \frac{1}{2}[a^{(1)}(\boldsymbol{x}) + a^{(2)}(\boldsymbol{x})], \quad \boldsymbol{x}\in\Omega\,. \tag{6.43}$$

We solve the weak form of FEM for $\tilde{u}_{\text{tail}}$ on Ω by

$$\int_\Omega \nabla\eta \cdot \nabla\tilde{u}_{\text{tail}}\, d\boldsymbol{x} + \int_\Omega \eta(a_{\text{tail}} + s_0^2)\tilde{u}_{\text{tail}}\, d\boldsymbol{x} = 0, \quad w_{\text{tail}} = \varphi(\boldsymbol{x}, s_0) \text{ on } \partial\Omega\,.$$

We compute the first guess for tails

$$\bar{v}_0(\boldsymbol{x}) = \frac{\bar{u}_0(\boldsymbol{x})}{s_0^2} = \frac{\ln \tilde{u}_{\text{tail}}}{s_0^2} \quad , \quad \boldsymbol{x} \in \Omega\,. \tag{6.44}$$

This tail $\bar{v}_0(\boldsymbol{x})$ is known as the first guess. By using $\bar{v}_0(\boldsymbol{x})$ as a tail function for the inverse problem, it has provided most of the information about locations of the inclusions. These locations were reconstructed precisely, and an iterative scheme similar to the steady-state problem was used to improve the contrast.

$$\Delta\tilde{u}_{i-1} - (a_{i-1} + s^2)\tilde{u}_{i-1} = -\delta(\boldsymbol{x} - \boldsymbol{x}_0)\,, \tag{6.45}$$

$$\Delta\tilde{u}_i - (a_i + s^2)\tilde{u}_i = -\delta(\boldsymbol{x} - \boldsymbol{x}_0)\,. \tag{6.46}$$

The difference of the above two equations can be written as follows

$$\Delta p_i - (a_i + s^2)p_i = (a_i - a_{i-1})\tilde{u}_{i-1}\,. \tag{6.47}$$

where $p_i = \tilde{u}_i - \tilde{u}_{i-1}$. The purpose of this iteration scheme is to improve the quality of $\tilde{u}(\boldsymbol{x}, \bar{s})$.

CHAPTER 7

GENERAL NUMERICAL IMPLEMENTATIONS

We have performed numerical experiments in 2D on several cases of reconstructions using the numerical methods discussed in chapters 5 and 6. We have chosen the range of geometrical parameters of the rectangle $\mathcal{A}$, which is typical for imaging of small animals and have chosen the range of optical parameters typical for biological tissues [11][1][19] and the range of thermal properties for biological tissue [20][21][22].

7.1 Domains

In our numerical simulation, according to our numerical method, we need to do the computing in three different types of domain, i.e., Ω_0, Ω and $\mathcal{A}$. We define these three domains in the following, see also figure 5.1, and use them for all examples.

– Domain $\mathcal{A}$, the domain of interest, is defined as

$$\mathcal{A} = \{(\boldsymbol{x}) = (x, y) : 6\text{cm} < x < 9\text{cm},\ 6\text{cm} < y < 14\text{cm}\}.$$

– Domain Ω, the computing domain for the inverse problem, is defined as

$$\Omega = \{(\boldsymbol{x}) = (x, y) : 5\text{cm} < x < 10\text{cm},\ 5\text{cm} < y < 15\text{cm}\}.$$

– Domain Ω_0, the simulating domain for the forward problem, is defined as

$$\Omega_0 = \{(\boldsymbol{x}) = (x, y) : 0\text{cm} < x < 15\text{cm},\ 0\text{cm} < y < 20\text{cm}\}.$$

Dimension of these three domains are clearly defined, the relation of them is $\mathcal{A} \subset \Omega \subset \Omega_0$. Our simulations are based on the assumptions that

(i) We assume that we know the background value of the coefficient inside the domain of interest, $\mathcal{A}$, but for the inclusions location and shape are unknown.

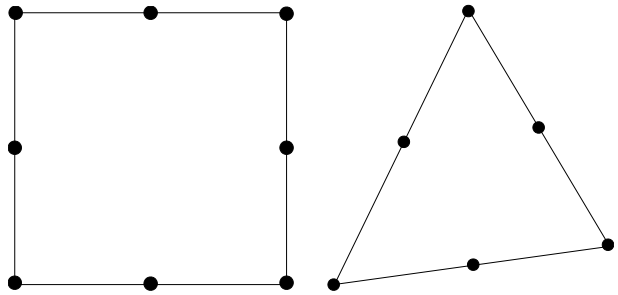

Figure 7.1. (a) Serendipity type of rectangular elements. (b) Quadratic triangular element.

(ii) For the domain $\Omega_0 \backslash \mathcal{A}$, we assume that we can fill in the matching media where its coefficients have the same properties as the background of $\mathcal{A}$.

(iii) Light or heat sources are merged into the matching media in $\Omega_0 - \mathcal{A}$ where their locations will be defined later in this section.

(iv) We can use the ICCD Camera to measure the light intensity on $\partial\mathcal{A}$ or an IR Camera to measure the heat intensity.

7.2 The Finite Element Mesh

In this study, we use a *serendipity type of rectangular elements*, see figure 7.1(a). The reason that we use rectangular elemenst is because of the tail problem. The serendipity type of rectangular element is selected because, bilinear type is not good for the high order equation and the other rectangular types with more points having a smooth high derivative which will take too much time for computation.

The details of the finite element mesh are required to be taken into account of the calculation. We know that the dense-grids usually give better results than the coarse-grid but the cost of computational time is another issue that we have to consider.

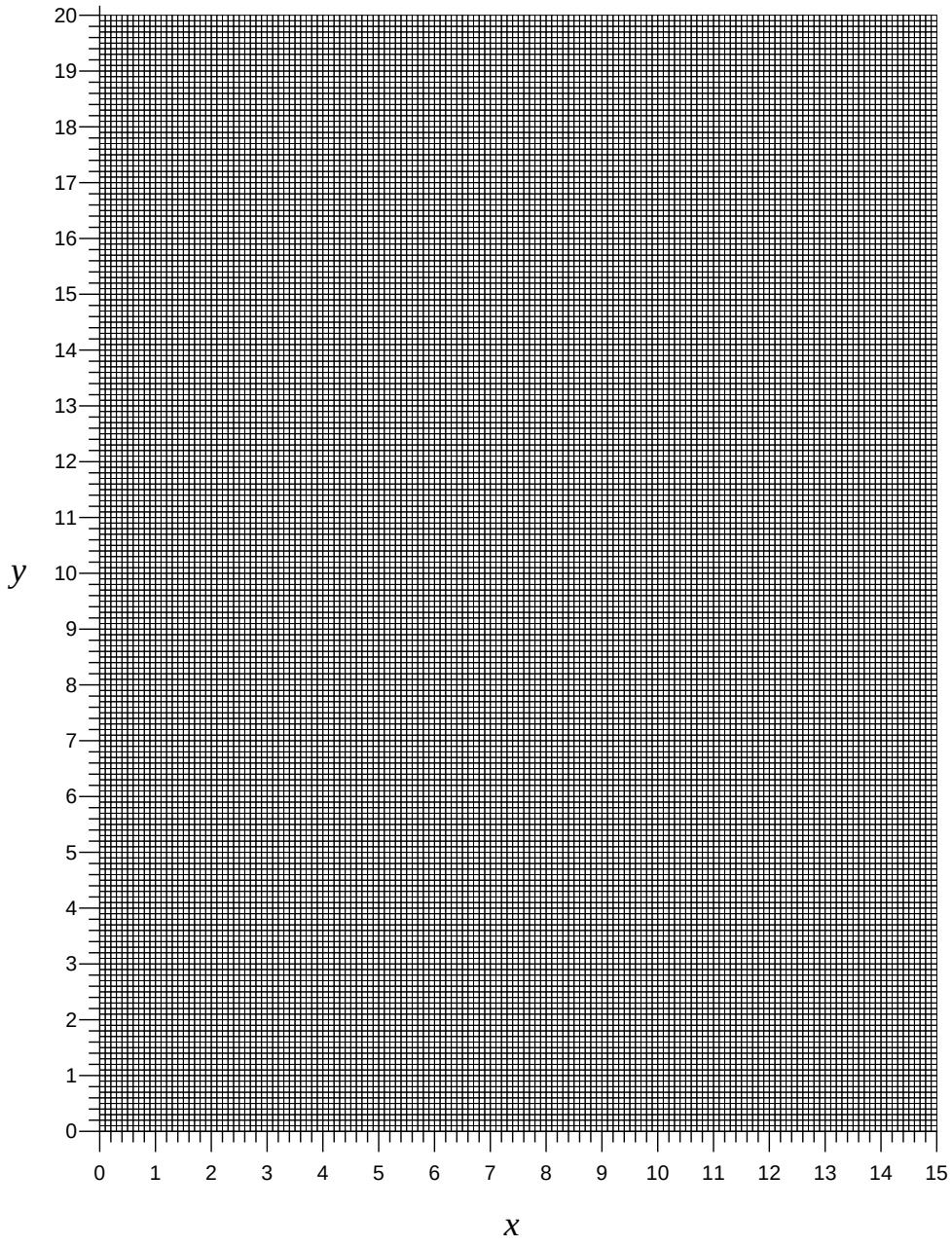

Figure 7.2. Domain mesh of Ω_0 (dense grid).

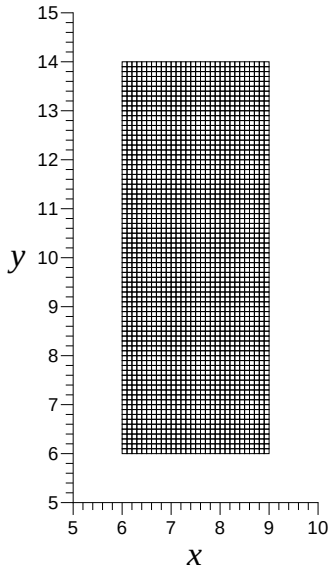

Figure 7.3. Domain mesh of $\mathcal{A}$ (dense grid).

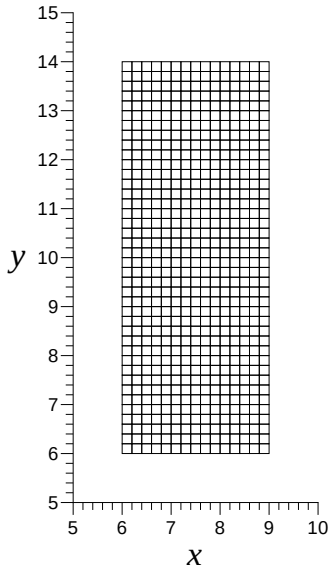

Figure 7.4. Domain mesh of $\mathcal{A}$ (coarse grid).

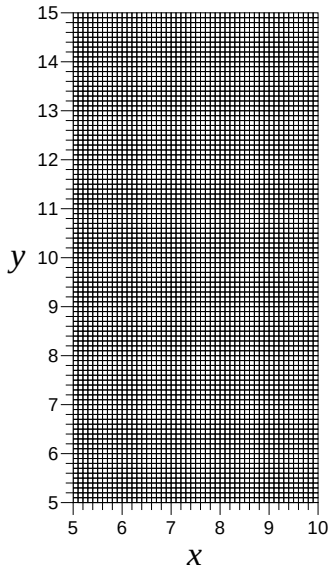

Figure 7.5. Domain mesh of Ω (dense grid).

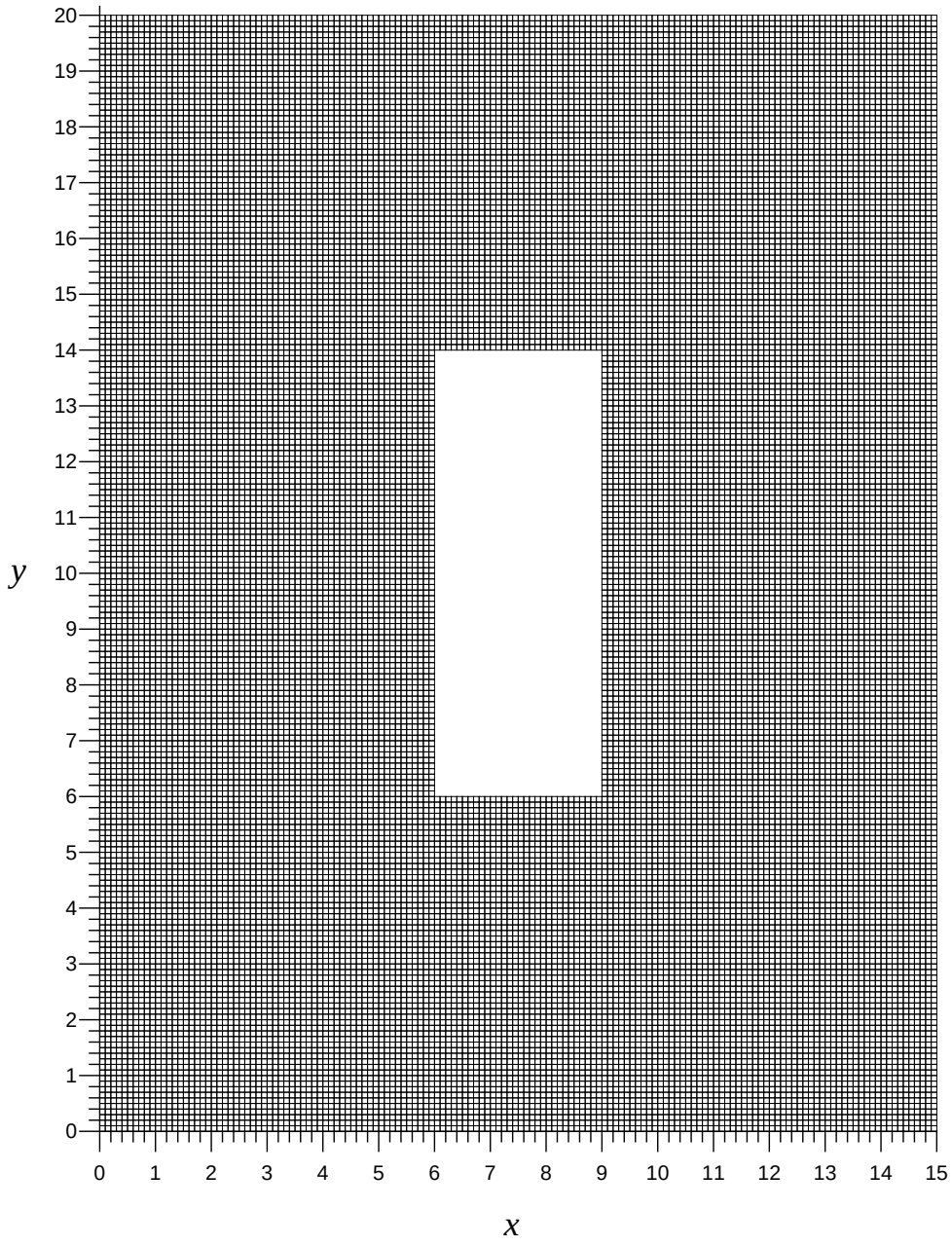

Figure 7.6. Domain mesh of $\Omega_0 - \mathcal{A}$ (dense grid).

First we show in our simulation the computation in dense-grid, total of 150×200, x, y direction, rectangular elements of Ω_0 is used for forward calculations, see figure 7.2. The total of 30×80 rectangular elements is used for the domain of interest $\mathcal{A}$, see figure 7.3, and 50×100 rectangular elements is used for computing domain Ω, see figure 7.5. Note that both $\mathcal{A}$ and Ω are sub domain of Ω_0. The number of measurement points on left, right, top and bottom of rectangular $\mathcal{A}$ are 161, 161, 61 and 61 respectively. The measurement points at the corners of rectangular are shared by each sides and therefore the total number of independent measuring points is 440.

There is another domain in our computation which is $\Omega_0 - \mathcal{A}$, see figure 7.6. This domain is used for the exterior forward problem. It has the same grid size as Ω_0, there are totally 27,600 elements in $(\Omega_0 - \mathcal{A})$.

CHAPTER 8

NUMERICAL IMPLEMENTATIONS AND RESULTS FOR THE STEADY-STATE PROBLEM

8.1 Heat Sources for the Steady State Problem

The heat sources are located in several positions $\boldsymbol{x}_0 = (12\text{cm}, s_i)$ along the left and $\boldsymbol{x}_0 = (3\text{cm}, s_i)$ along the right hand side of the rectangle $\mathcal{A}$ (in domain Ω_0). In our simulations, we have used an ideal heat source modeled by the function $-\delta(\boldsymbol{x} - \boldsymbol{x}_0)$ in the 2D case of (1.6). In numerical simulation $\delta(\boldsymbol{x} - \boldsymbol{x}_0) = c\eta(\boldsymbol{x})$, where η is the finite element at the location and c is the scaling constant to ensure that the integral of δ in Ω_0 equal one.

In our setting, we use totally fourteen heat sources to generate the measurement. Let's denote s_i as a representation of light source. The measurement data from light sources s_i, $i = 0, 1, 2, 3, 4$ located above and right of $\mathcal{A}$, first three, 3, are used for computation of tail from angle#1 and all five, 5, are used for the inverse problem. The heat sources s_i, $i = 5, 6, 7$ located below and right of $\mathcal{A}$ are use for computation of tail from angle#2. The heat sources s_i, $i = 8, 9, 10$ located above and left of $\mathcal{A}$ are used for computation of tail from angle#3. And lastly, the heat sources s_i, $i = 11, 12, 13$ located below and left of $\mathcal{A}$ are used for computation of tail from angle#4, see figure 8.1. Note that, only heat sources s_i, $i = 0, 1, 2, 3, 4$, are used for the inverse problem, parameter B in $\boldsymbol{x}_0 = (B, s)$ is the fixed location of $\boldsymbol{x}$ for these heat sources.

The value of s_i's are numerically show as follows

$$s_0 = 17\text{cm},\ s_i = s_{i-1} - 0.2\text{cm},\ i = 1, 2, 3, 4\,,$$

$$s_5 = 3\text{cm},\ s_i = s_{i-1} + 0.2\text{cm},\ i = 6, 7\,,$$

$$s_8 = 17\text{cm},\ \ s_i = s_{i-1} - 0.2\text{cm},\ \ i = 9, 10 \qquad \text{and}$$

$$s_{11} = 3\text{cm},\ \ s_i = s_{i-1} + 0.2\text{cm},\ \ i = 12, 13\,,$$

where $\boldsymbol{x}_0 = (B, s_i)$, $i = 0, \ldots, 7$ for heat source on the right of $\mathcal{A}$ and $\boldsymbol{x}_0 = (\tilde{B}, s_i)$, $i = 8, \ldots, 13$ for heat source on the left of $\mathcal{A}$. We set $B = 12\text{cm}$ and $\tilde{B} = 3\text{cm}$.

In fact, these value of s_i's cannot be set too large because the limitation of the size of space and the location of heat source which cannot be located too far from $\mathcal{A}$.

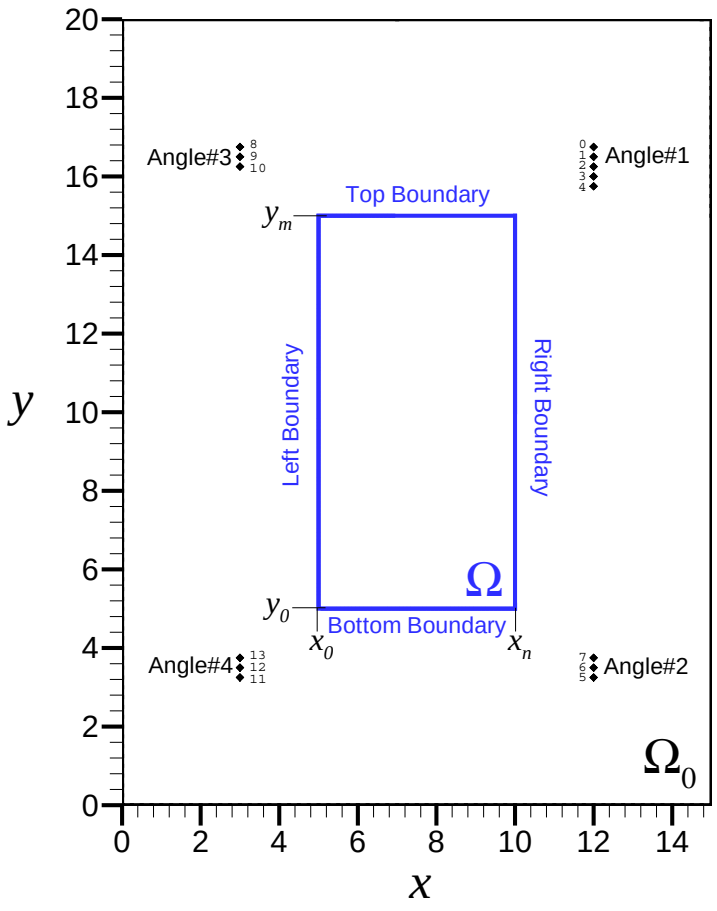

Figure 8.1. A domain with fourteen source locations.

8.2 Numerical Results for Thermal Tomography

The GCM method has found great application in diffusive optical tomography. Another application of this type of globally convergent inverse problem is proposed for thermal tomography. In recent studies [20][21][22] authors have shown these temperature distribution changes are directly linked with formation of blood clots in brain. With a small clot in a animal model, a detectable temperature drop of near one half degree was observed. One of the direct applications of GCM, will be reconstruction in thermal tomography.

In thermal tomography, as indicated before, we hope to reconstruct the distribution of blood perfusion coefficient inside brain. In this section, we use simulated thermal data to reconstruct perfusion distribution using the GCM algorithm. The physical parameters of the simulation are in the realistic range.

In figure (8.2), we provide the forward problem with two inclusions of 0.65cm radius. We find if the background α value of 0.00001 is close to the thermal measurement data of a small mammal at 36.9 degrees Celcius. The difference of temperature with/without two 0.65cm radius inclusions will be about 0.2 degrees. This background α value of 0.00001 is considered low by common standard, but it is fitting for brain model where blood metabolic heat is low and the concentration of blood is very low in most regions.

8.2.1 Example

We consider a case of thermal tomography. The physical domain is a rectangle. The coefficient $a(\boldsymbol{x}) = 0.005$ inside of inclusions and $a(\boldsymbol{x}) = 0.00001$ outside of inclusions. These coefficients were chosen based upon their effect of the forward model without an additional heat source. From a practical standpoint since the metabolic heat generated is being ignored, these coefficient levels demonstrated, after effect of

adding two inclusions, are limited to only decreasing the body's temperature by 0.2 degrees Celsius, see figure (8.2a). The amplitude of the heat source is kept minimal to not allow any discomfort, see figure (8.2b).

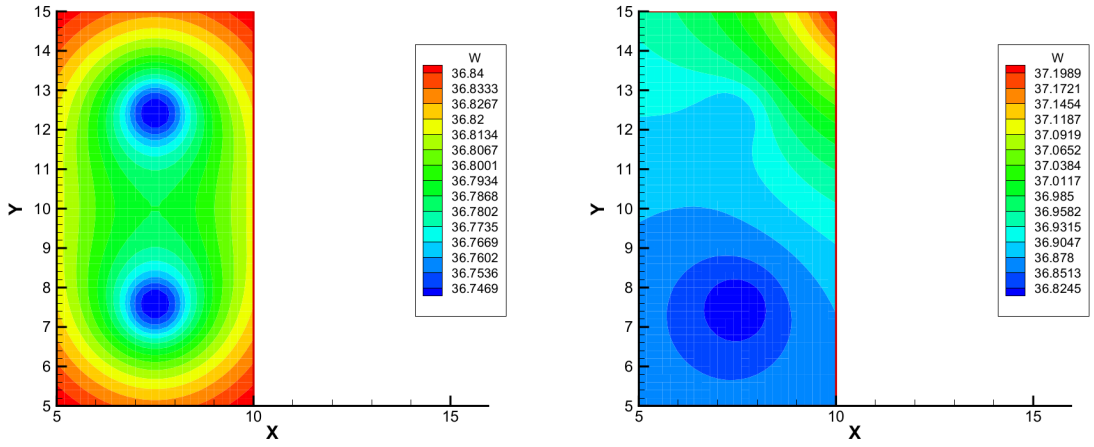

(a) (b)

Figure 8.2. (a) Two Inclusions are at (7.5cm, 7.5cm) and (7.5cm, 12.5cm). The temperature distribution is shown. (b)We show the temperature distribution of with one additional heat source in the upper-right corner.

The levels of this coefficient are inconsistent with what most physicians would consider to be appropriate levels of perfusion in a normal brain, however since the metabolic heat was removed from the equation because of stroke, lower levels of this coefficient are assumed. As has been noticed in previous mathematical models [23] blood perfusion has a cooling effect upon the tissue once the temperature reaches a state of equilibrium. Our model is based upon the assumption that the temperature of the flesh and the heat source have reached a state of equilibrium.

In figure (8.3b), we show an example of reconstruction using the GCM discussed earlier. Figure (8.3) contains 2 inclusions located at $(7.5\text{cm}, 7.5\text{cm})$ and $(7.5\text{cm}, 12.5\text{cm})$ with a radius of 0.65cm where $a(x) = 0.005$.

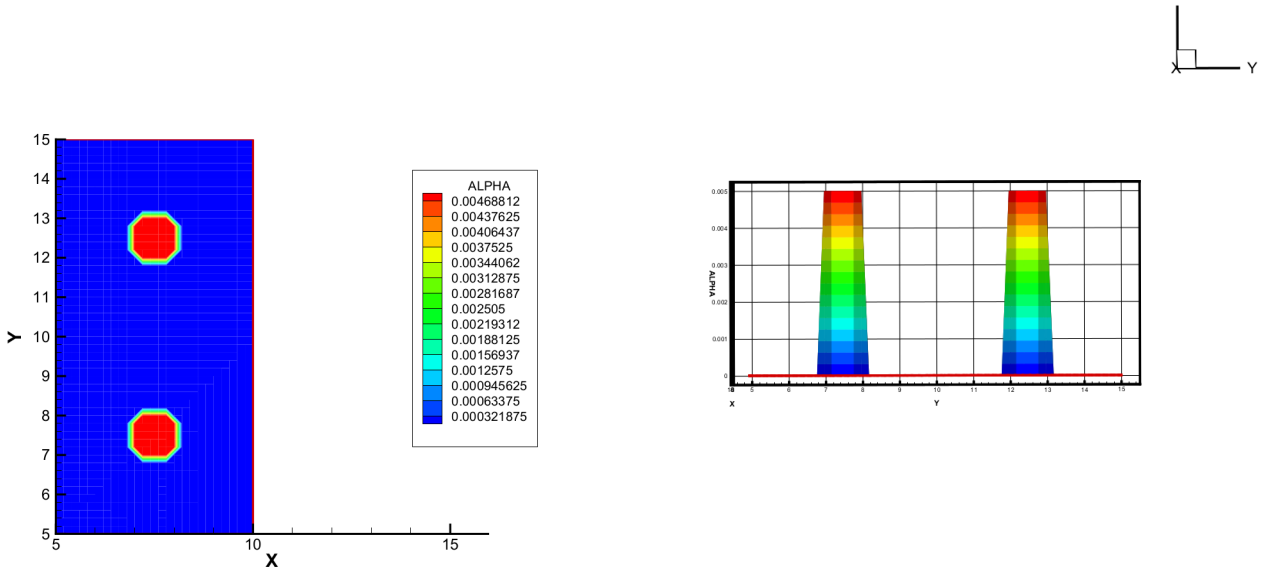

(a)

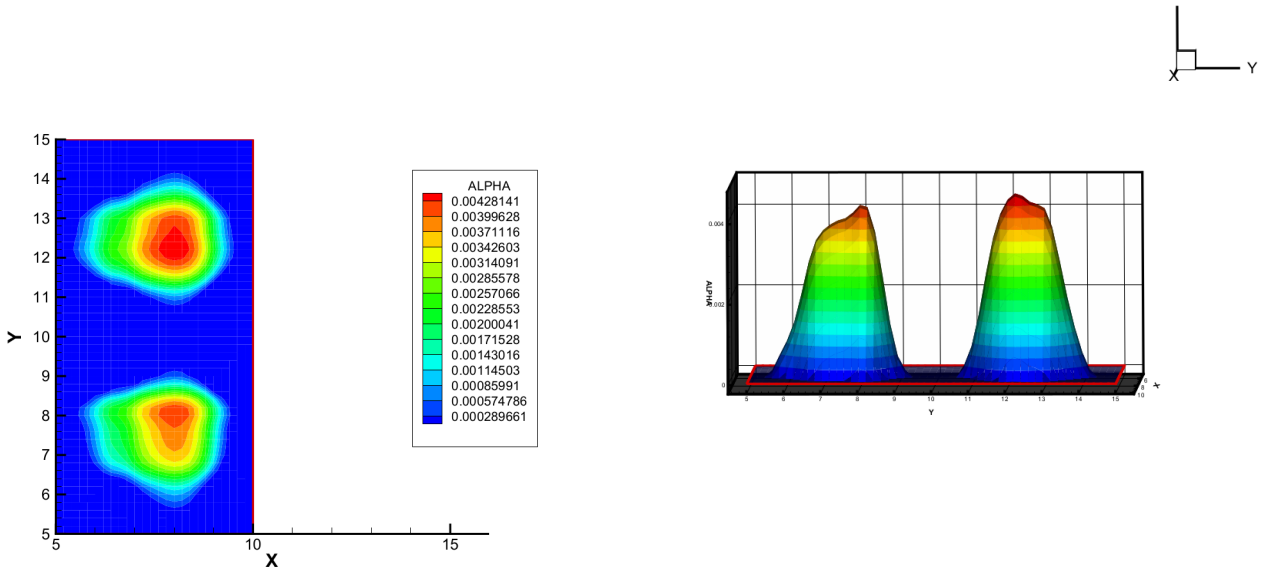

(b)

Figure 8.3. (a) A display of the original coefficient $a(\boldsymbol{x})$ of figure (8.2) for the Steady-State Problem. (b) Inverse problem reconstruction result using 10% of the total difference of temperature as the noise level.

The relative errors of the reconstruction which are Root-Mean-Square-Error (RMSE), Absolute-Mean-Error (AME) and Relative Mean-Error (ME) are calculated as follows

$$\text{RMSE} = \frac{\sqrt{\sum_{k=1}^{N^{(\text{node})}} (a_k - \hat{a}_k)^2}}{N^{(\text{node})} \max_k |a_k|} \quad , \quad \text{AME} = \frac{\sum_{k=1}^{N^{(\text{node})}} |a_k - \hat{a}_k|}{N^{(\text{node})} \max_k |a_k|} \quad ,$$

$$\text{ME} = \frac{\sum_{k=1}^{N^{(\text{node})}} (a_k - \hat{a}_k)}{N^{(\text{node})} \max_k |a_k|} \, . \tag{8.1}$$

Note that $\{a_1, \ldots, a_{N^{(\text{node})}}\}$ are the original distribution data in Ω and $\{\hat{a}_1, \ldots, \hat{a}_{N^{\text{node}}}\}$ are its approximation, the values of them are taken at each of the grid points of the computation domain Ω, $N^{(\text{node})}$ is the total number of nodes in domain Ω.

Table 8.1. Error Results for the Steady-State Problem

ERROR	METHOD
0.357863384987837	RMSE
0.245956183503438	AME
-0.191183462237716	ME

Table 8.2. Computation Time for the Steady-State Problem

COMPUTATION TIME FOR INVERSE PROBLEM
18 MIN 09 SEC

CHAPTER 9

NUMERICAL IMPLEMENTATIONS AND RESULTS FOR THE TIME-DEPENDENT PROBLEM

9.1 Light Sources for the Time-Dependent Problem

For the time-dependent optical tomography problem the major achievement is the ability to limit the number of light sources. From an engineering standpoint this is desirable to limit the number of experiments and calibration of equipment. Instead of having fourteen different positions which would require fourteen different experiments our simulations for the time-dependent problem only require two source positions and then uses changes in the psuedo-frequencies for the inverse problem instead of changes in the source position. The source positions are located in the upper right, $\boldsymbol{x}_0 = (12, 17)$, and lower left, $\boldsymbol{x}_0 = (3, 3)$, portions of the domain.

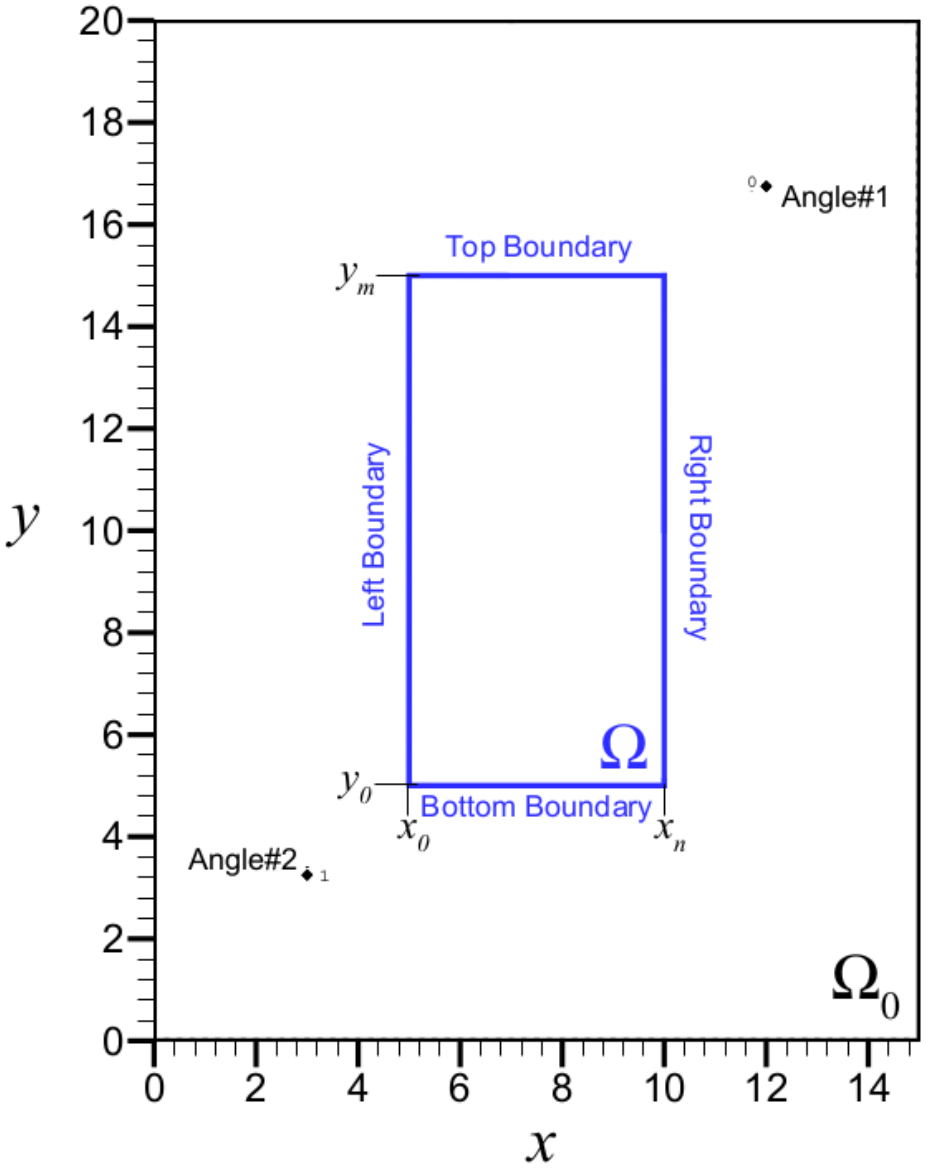

Figure 9.1. A domain with two source locations.

9.2 Numerical Results for Time-Dependent Optical Tomography

The GCM method has found great application in steady state diffusive optical tomography. The application of this current globally convergent inverse problem is proposed for the time-dependent optical tomography problem.

In optical tomography, as indicated before, we hope to reconstruct the distribution of the absorption coefficient inside the brain. In this section, we use simulated optical data to reconstruct absorption distribution using the GCM algorithm. The physical parameters of the simulation are in the realistic range for rat brains.

9.2.1 Example

We consider a case of optical tomography. The physical domain is a rectangle. The coefficient $a(\boldsymbol{x}) = 3.24$ inside of inclusions and $a(\boldsymbol{x}) = 1.08$ outside of inclusions. Instead of altering source positions along a line located outside of Ω but in Ω_0, a single source position is fixed and the pseudo-frequency is altered. Reconstruction from a single source position leads to inaccuracies in the target coefficient. In this case only two source positions were used. One located to the upper right and one to the lower left of Ω.

The pseudo-frequencies used for the reconstruction are chosen by testing a broader spectrum of frequencies and then refining that spectrum to the appropriate levels by focusing on reconstructions with the lowest contrast while still carrying information about the target coefficient. The reconstruction actually recovers $a(\boldsymbol{x}) + s^2$. So to get the original coefficient the only extra step is to subtract s^2 from all of the nodal points. The frequencies used were [1.70,1.71,...,1.89].

In figure (9.2b), we show an example of reconstruction using the GCM discussed earlier. Figure 9.2 contains 2 inclusions located at (7.5cm, 7.5cm) and (7.5cm, 12.5cm) with a radius of 0.65cm.

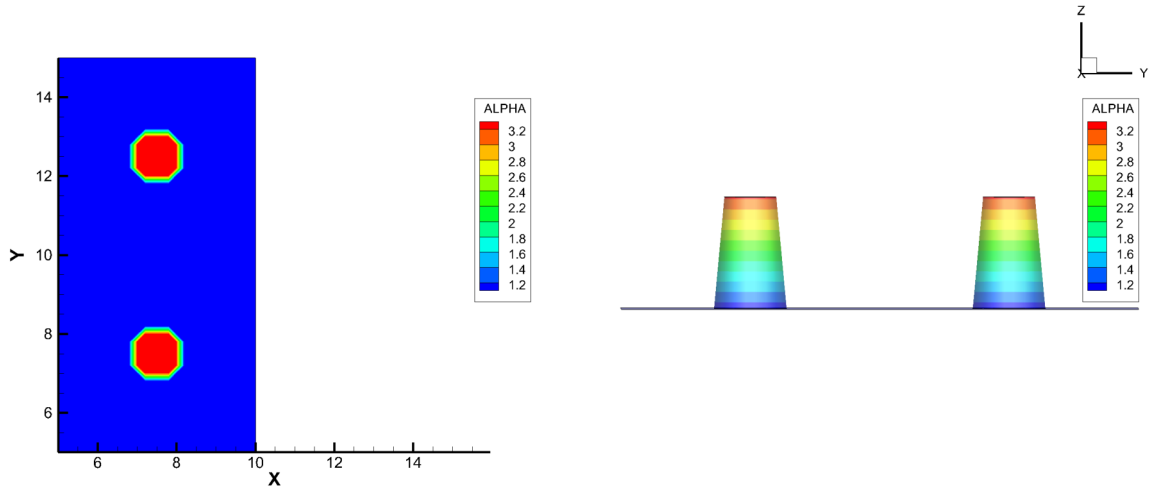

(a)

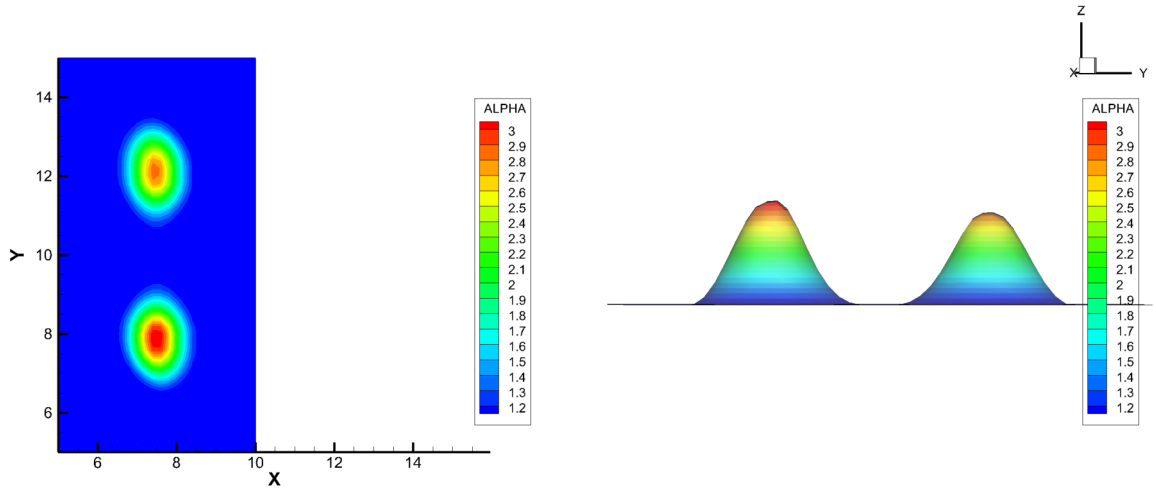

(b)

Figure 9.2. (a) A display of the original coefficient $a(\boldsymbol{x})$ for Example 1 of the Time-Dependent Problem. (b) Inverse problem reconstruction using 5% as the noise level..

Table 9.1. Error Results for Example 1 of the Time-Dependent Problem

TAIL	RMSE	AME	ME
Distant Tail	0.111058548016803	0.032093788026051	0.008822377977849
Rescaled Tail	0.158675407685139	0.065514320821362	0.018009469644997

Table 9.2. Computation Time for Example 1 of the Time-Dependent Problem

TAIL	COMPUTATION TIME FOR INVERSE PROBLEM
Distant Tail	17 MIN 59 SEC
Rescaled Tail	17 MIN 40 SEC

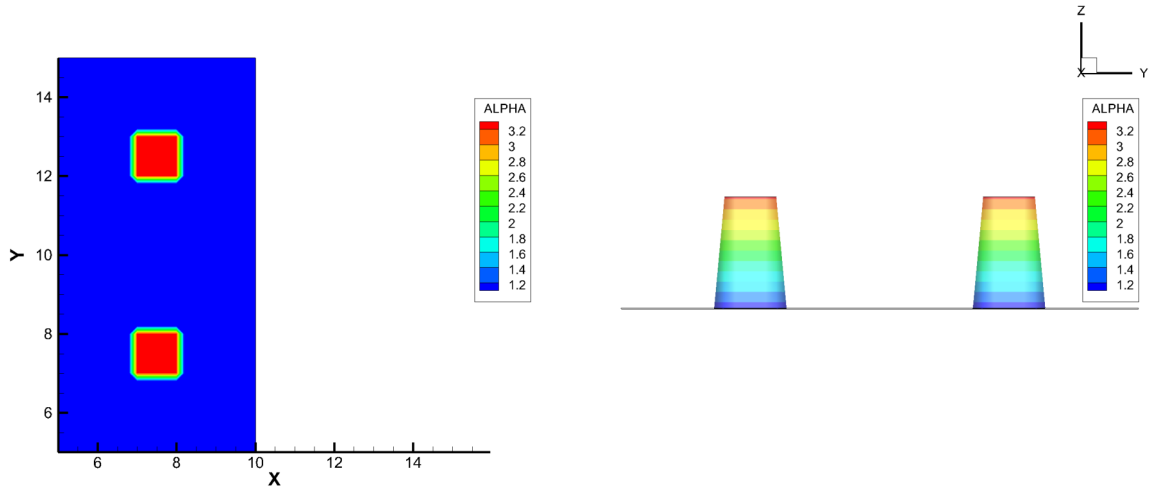

(a)

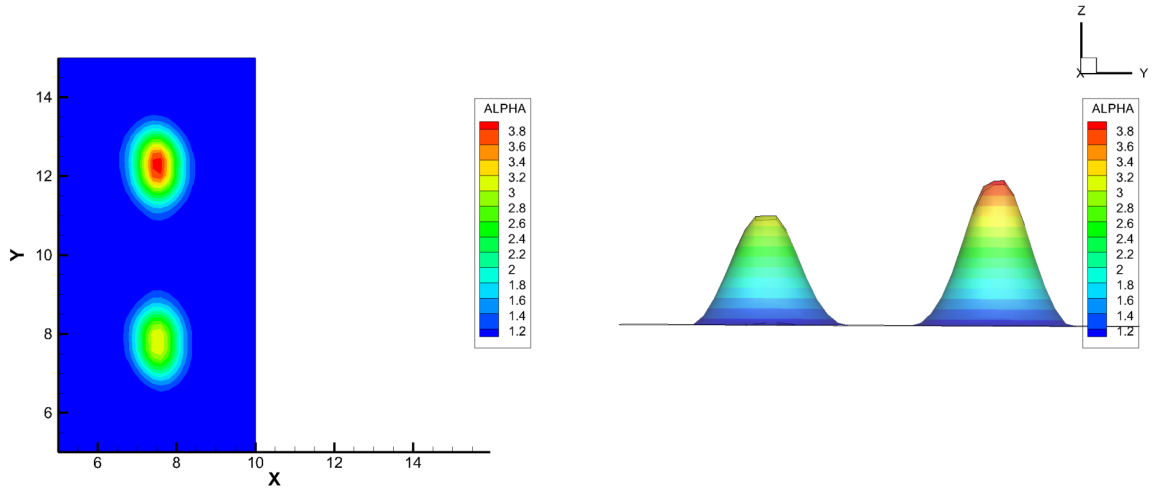

(b)

Figure 9.3. (a) A display of the original coefficient $a(\boldsymbol{x})$ for Example 2 of the Time-Dependent Problem. (b) Inverse problem reconstruction result using 5% as the noise level.

Table 9.3. Error Results for Example 2 of the Time-Dependent Problem

TAIL	RMSE	AME	ME
Distant Tail	0.106509360602857	0.030841897210781	0.006599397899766
Rescaled Tail	0.154606269885120	0.061956265480062	0.010494501696482

Table 9.4. Computation Time for Example 2 of the Time-Dependent Problem

TAIL	COMPUTATION TIME FOR INVERSE PROBLEM
Distant Tail	25 MIN 15 SEC
Rescaled Tail	22 MIN 55 SEC

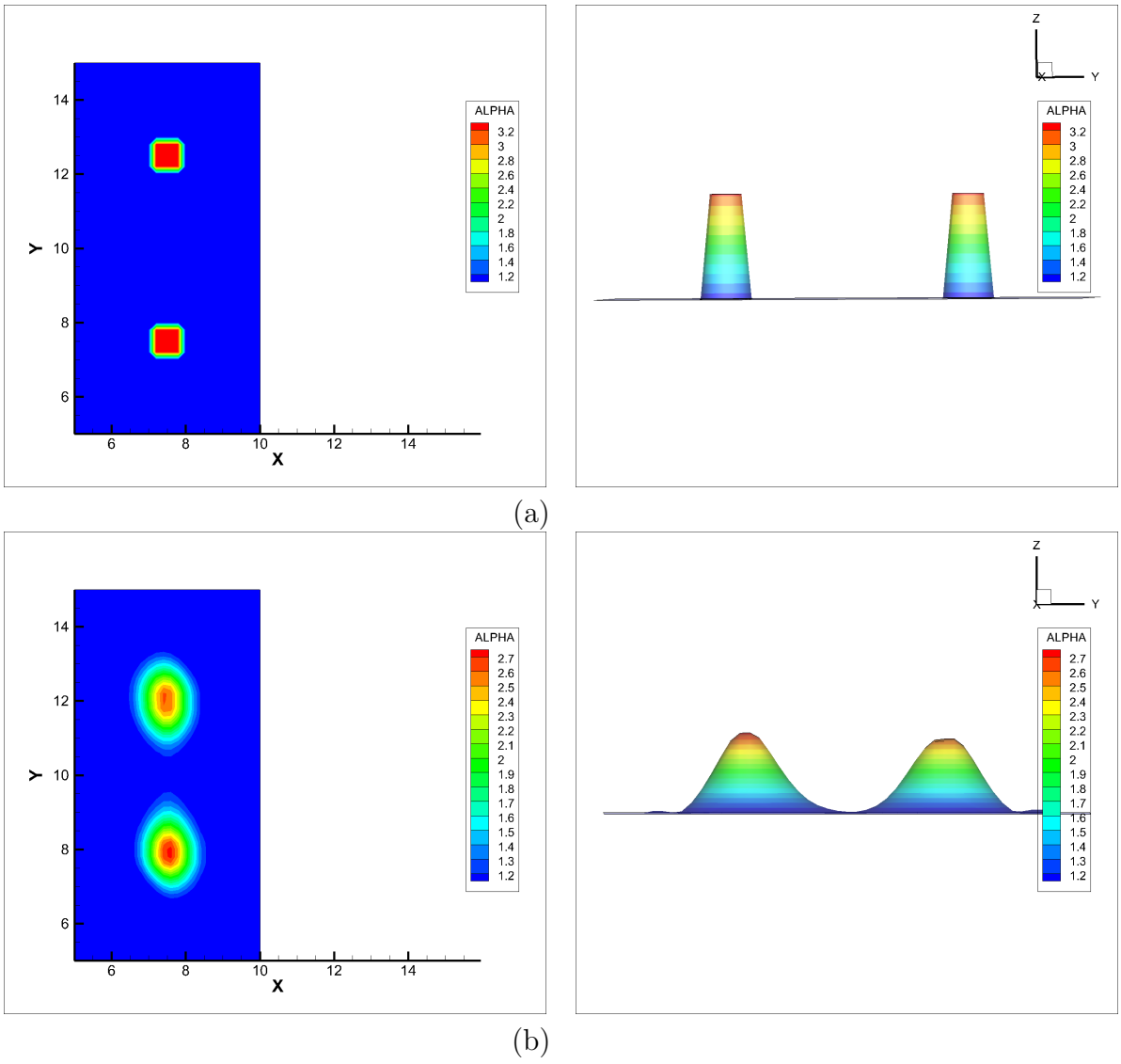

Figure 9.4. (a) A display of the original coefficient $a(\boldsymbol{x})$ for Example 3 of the Time-Dependent Problem. (b) Inverse problem reconstruction result using 5% as the noise level.

Table 9.5. Error Results for Example 3 of the Time-Dependent Problem

TAIL	RMSE	AME	ME
Distant Tail	0.096744243770225	0.028385822192094	-0.001954882007734
Rescaled Tail	0.140966616611940	0.056881495124859	-0.004731051705342

Table 9.6. Computation Time for Example 3 of the Time-Dependent Problem

TAIL	COMPUTATION TIME FOR INVERSE PROBLEM
Distant Tail	25 MIN 41 SEC
Rescaled Tail	25 MIN 21 SEC

CHAPTER 10

CONCLUSIONS AND DISCUSSION

Our numerical experiments indicated that this method, globally convergent method (GCM), is quite stable. Computation results show a good performance for a realistic range of parameters in two separate physical problems. In this dissertation, we study (GCR) as a useful tool for reconstruction of the range of thermal parameters typical for biological tissue [20][21][22] and of optical parameters typical for biological tissues [1][11][19] incorporating time-dependent data.

We used the continuous piecewise linear function as approximate and find they have approximated well and we get a good reconstruction image from simulated time-domain and steady-state data.

Two different "Tail Functions" were incorporated in the time-dependent problem each of which is based on a different assumption about the nature of the problem. The first assumes that the source position is far enough away that the forward solution will resemble the uniform solution without any inclusions. In fact from any engineering standpoint this is impractical since a source position infinitely far away would provide no information about the problem.

After rescaling the domain to get a tail function the assumption is that the psuedo-frequency is large enough to achieve asymptotic behavior allowing the source position to be close to the physical domain. From a theoretical and numerical standpoint this is impractical since we can not really make the frequencies that large however this tail function matches the physical reality of the problem more closely.

After using both tail functions the rescaled tail function had a slightly faster computational rate for all reconstructions however there was a slightly higher error versus the original tail function.

10.1 Acknowledgement

This work is partially supported by the NIH grant, # $4R33NS05285003$, the GAANN Program, and the GK-12 Program.

REFERENCES

[1] S. Arridge, "Optical tomography in medical imaging," *Inverse Problems*, vol. 15, pp. 841–893, 1999.

[2] A. B. Bakushinsky, T. Khan, and A. Smirnova, "Inverse problem in optical tomography and its numerical investigation by iteratively regularized methods," *J. Inv. Ill-Posed Problems*, vol. 13, pp. 537–551, 2005.

[3] Yu. A. Grazin, M. V. Klibanov, and T. R. Lucas, "Numerical solution of a subsurface imaging inverse problem," *SIAM J. Appl. Math.*, vol. 62, pp. 664–683, 2001.

[4] E. Haber, U. M. Asher, and D. Oldenburg, "On optimization techniques for solving nonlinear inverse problems," *Inverse Problems*, vol. 16, pp. 1263–1280, 2000.

[5] M. V. Klibanov and A. Timonov, *Carleman Estimates for Coefficient Inverse Problems and Numerical Applications*. Utrecht: VSP, 2004.

[6] H. Shan, M. V. Klibanov, N. Pantong, J. Su, and H. Liu, "A globally accelerated numerical method for optical tomography with continuous wave source," *J. Inv. Ill-Posed Problems*, vol. 16, pp. 765–792, 2008.

[7] N. Pantong, J. Su, H. Shan, M. V. Klibanov, and H. Liu, "Globally accelerated reconstruction algorithm for diffusion tomography with continuous-wave source in an arbitrary convex shape domain," *J. Optical Society of America A*, vol. 26, pp. 456–472, 2009.

[8] H. Shan, M. V. Klibanov, H. Liu, N. Pantong, and J. Su, "Numerical implementation of the convexification algorithm for an optical diffusion tomograph," *Inverse Problems*, vol. 24, p. 025006, 2008.

[9] M. V. Klibanov, J. Su, N. Pantong, H. Shan, and H. Liu, "A globally convergent numerical method for an inverse elliptic problem of optical tomography," *J. Applicable Analysis*, vol. 89, no. 6, pp. 861–891, 2010.

[10] L. Beilina and M. Klibanov, "Reconstruction of dielectrics from experimental data via a hybrid globally convergent/adaptive inverse algorithm," *Inverse Problems (26)*, 2010.

[11] R. R. Alfano, R. R. Pradhan, , and G. C. Tang, "Optical spectroscopic diagnosis of cancer and normal breast tissues," *J. Opt. Soc. Am.*, vol. B 6, pp. 1015–1023, 1989.

[12] S. Arridge and J. Schotland, "Optical tomography: Forward and inverse problems," *Topical Review Inverse Problems (25)*, 2009.

[13] H. H. Pennes, "Analysis of tissue and arterial blood temperatures in the resting human forearm," *Journal of Applied Physiology*, vol. 1, pp. 93–122, 1948.

[14] E. H. Wissler, "Pennes' 1948 paper revisited," *Journal of Applied Physiology*, vol. 85, pp. 31–41, 1998.

[15] L. Beilina and M. V. Klibanov, "A globally convergent numerical method for a coefficient inverse problem," *SIAM J. Sci. Comp.*, vol. 31, pp. 478–509, 2008.

[16] O. A. Ladyzhenskaya and N. N. Uralceva, *Linear and Quasilinear Elliptic Equations*. New York: Academic Press, 1969.

[17] S. I. Kabanikhin, A. D. Satybaev, and M. A. Shishlenin, *Direct Methods of Solving Multidimensional Inverse Hyperbolic Problems*. Utrecht: VSP, 2004.

[18] L. C. Evans, *Partial Differential Equations*. American Mathematical Society, 1998.

[19] D. Grosenick, H. Wabnitz, H. H. Rinneberg, K. T. Moesta, and P. M. Schlag, "Development of a time-domain optical mammograph and first in vivo applications," *Applied Optics*, vol. 38, pp. 2827–2943, 1999.

[20] E. A. Kiyatkin, "Brain hyperthemia as physiological and pathological phenomena," *Brain Research Reviews*, vol. 50, pp. 27–56, 2005.

[21] C. Diao, L. Zhu, and H. Wang, "Cooling and rewarming for brain ischemia or injury: Theoretical analysis," *Annals of Biomedical Engineering*, vol. 31, pp. 346–353, 2003.

[22] R. Busto, W. Dietric, M. Globusand, I. Valedes, P. Scheinberg, and M. Ginsberg, "Small differences in intraischemic brain temperature critically determine the extent of ischemic neuronal injury," *Journal of Cerebral Blood Flow and Metabolism*, vol. 7, pp. 729–738, 1987.

[23] P.-J. Cheng and K.-C. Liu, "Numerical analysis of bio-heat transfer in a spherical tissue," *Journal of Applied Sciences*, vol. 9, pp. 962–967, 2009.

BIOGRAPHICAL STATEMENT

Aubrey Rhoden was born in Waco, Texas in 1984. He received his B.S. degree in Mathematics from Texas State University, San Marcos, Texas in 2007. After graduating from Texas State he joined the University of Texas at Arlington's Graduate Mathematics Program where he received his Ph. D. in Applied Mathematics in May of 2013. During his years in graduate school he was a graduate teaching assistant, GAANN Fellow, and a GK-12 Fellow. During graduate school he also was married to his wife, Ginna, and had a daughter, Jude. He was also a member of the Society for Industrial and Applied Mathematics (SIAM) and the American Mathematical Society (AMS). His research interests include partial differential equations, inverse problems, and numerical analysis.